Precambrian Research 366 (2021) 106416

Contents lists available at ScienceDirect

Precambrian Research

journal homepage: www.elsevier.com/locate/precamres

Origin of K-bentonites in the Doushantuo cap dolostones from South China and its potential link with the sedimentary model of the Marinoan cap dolostones

Mingzhong Zhou [a,b,*], Bin Wan [c], Li Zhou [a,b], Enlin Yang [a,b], Liansheng Yang [a,b], Taiyi Luo [d,*]

[a] School of Geographical and Environmental Sciences, Guizhou Normal University, Guiyang 550001, China
[b] State Key Laboratory Incubation Base for Karst Mountain Ecology Environment of Guizhou Province, Guiyang 550001, China
[c] State Key Laboratory of Palaeobiology and Stratigraphy, Nanjing Institute of Geology and Palaeontology, Chinese Academy of Sciences, Nanjing 210008, China
[d] State Key Laboratory of Ore Deposit Geochemistry, Institute of Geochemistry, Chinese Academy of Sciences, Guiyang 550002, China

ARTICLE INFO

Keywords:
Jiuqunao section
Heyu section
K-bentonite
Marinoan cap dolostone
Snowball Earth

ABSTRACT

A study of the K-bentonites in the Doushantuo cap dolostones on the Yangtze Platform in South China would facilitate understanding the origin of the Marinoan cap dolostones and testing the snowball Earth hypothesis. To date, sporadic work has been conducted on the whole-rock geochemistry of the K-bentonites from the platform and slope of the Yangtze Platform, to preliminarily understand the genesis of the K-bentonites. However, a study of the whole-rock geochemistry of the K-bentonites from the basin and on zircon geochemistry of the K-bentonites from the entire Yangtze Platform has not been carried out. Therefore, the nature of the primary magmas, source and tectonic setting of the source volcanoes, and the episodes of source volcanic eruptions of the K-bentonites are unknown, which hinders unraveling the possible link between the sedimentary model of the Marinoan cap dolostone and the K-bentonites. Here, we perform a systematic study of the whole-rock and zircon geochemistry of the K-bentonites. The major and trace element concentrations of the K-bentonites and trace element contents in their volcanic zircons suggest that the primary magmas of the K-bentonites from the Jiuqunao and Heyu sections are different in nature. The same geochemical results indicate that the source volcanoes of all the K-bentonites may occur in the extensional setting on the northern margin of the Yangtze Block. Hf isotopic compositions of the volcanic zircons in the K-bentonites imply that the source magmas of the K-bentonites are mainly mantle-derived, and may have mixed with the crustal materials from the northern margin of the Yangtze Block. Based on the difference in whole-rock and zircon geochemistry of the K-bentonites from Heyu and Jiuqunao, two episodes of the source volcanic eruptions of the K-bentonites could be identified. The K-bentonite at Heyu most probably represents the record of the old episode, while that at Jiuqunao represents the record of the young one. The here proposed dual episodic deposition of K-bentonites within the Doushantuo cap carbonates holds potential significance to constrain 1) the duration of the cap carbonate deposition and 2) their genesis in potential slushball or snowball Earth environments.

1. Introduction

The widely exposed cap dolostone (known as the Doushantuo cap dolostone) overlying the Nantuo (Marinoan) glacial diamictite in South China, is one of the important windows for unraveling the most severe paleoclimatic event during the terminal Neoproterozoic. However, it is still widely debated whether the glaciation was global in its extent and a slushball Earth hypothesis has been proposed (Hyde et al., 2000; Shields, 2005; Lewis et al., 2007; Micheels and Montenari, 2008; Allen and Etienne, 2008). The snowball Earth hypothesis (SEH), which was first proposed by Kirschvink (1992), and then has been substantially developed by Hoffman et al. (1998), is one candidate for explaining the genesis of the Marinoan glacial deposits that sprawled to the low-latitude zones of the Earth. According to the SEH, the entire Earth was covered by ice sheet during the Marinoan galaciation. Subsequently, the long-term accumulation of CO_2 caused by volcanic activities made the atmospheric CO_2 concentration about 350 times higher than that of today. The greenhouse effect caused by CO_2 on the Earth eventually led

* Corresponding authors at: School of Geographical and Environmental Sciences, Guizhou Normal University, Guiyang 550001, China (M. Zhou).
E-mail addresses: mingzhongzhou@126.com (M. Zhou), luotaiyi@vip.gyig.ac.cn (T. Luo).

https://doi.org/10.1016/j.precamres.2021.106416
Received 19 July 2021; Received in revised form 22 September 2021; Accepted 27 September 2021
Available online 14 October 2021

to the melting of the ice sheet and the rapid deposition of the cap dolostone. Therefore, the genetic model for the Marinoan cap dolostone plays a crucial role in testing the SEH.

The genesis of Marinoan cap dolostones is still highly debated. Shields (2005) and Hohl et al. (2017) have summarized the main models as follows: (1) overturn and widespread upwelling of anoxic and organic carbon-rich deep oceanic water masses and oxidation of the latter (Grotzinger and Knoll, 1995); (2) highly accelerated weathering rates during greenhouse conditions after the snowball Earth event that led to an increase in seawater alkalinity and thus increased carbonate precipitation during transgressional periods (Kirschvink 1992; Hoffman et al. 1998; Spence et al., 2016); (3) oxidation of a large ^{12}C-enriched pool of organic carbon (e.g. gas hydrates from permafrost soils) (Kennedy et al. 2001; Jiang et al. 2003); (4) abrupt deglaciation leading to the formation of a stratified ocean with a huge freshwater lens on the surface formed from meltwaters and the fast precipitation of cap dolomites (Shields, 2005).

At present, there are mainly three possible models for the sedimentary sequence of the Marinoan cap dolostones from deep- to shallow-water facies (Fig. 1), and each model carries a different implication for the timescale of the cap dolostones, and therefore for their origin (Hoffman et al., 2007). The first model considers that the base and top of the cap dolostones in different facies are approximately isochronous (Jiang et al., 2006), thus the timescale of the cap dolostones is not limited by the ice-sheet meltdown time (Fig. 1A). The second model holds that the bases of the cap dolostones in different facies are diachronous, but their tops are isochronous, and therefore the timescale of cap dolostones is also not limited by the ice-sheet meltdown time (Fig. 1B). The third model claims that the bases and tops of the cap dolostones are diachronous (Hoffman et al., 2007), hence the timescale of the cap dolostones at any section is less than the ice-sheet meltdown time (Fig. 1C).

K-bentonite is formed from volcanic ashes or tuffaceous materials which were deposited in the marine environment through a series of geological processes including hydrolysis, diagenesis, and even low-grade metamorphism (Su et al., 2009; Su et al., 2008; Zhou et al., 2014; Huff, 2016; Zhou et al., 2018; Xu et al., 2020). Through initial geological process, volcanic ashes or tuffaceous materials transferred to bentonite consisting mainly of smectites. Then through long diagenesis or even low-grade metamorphism the bentonite transferred to K-bentonite, which is composed mainly of potassium-bearing clay minerals such as illite and mixed-layer illite–smectite (Fang et al., 2017; Gong et al., 2018; Hong et al., 2019a, Hong et al., 2019b). Thus, K-bentonite has a higher K_2O content as compared with traditional bentonite which is dominated by montmorillonite (Zhou et al., 2014). Generally, the K_2O content of K-bentonite is higher than 3%, while that of traditional bentonite is lower than 1% (Zhou et al., 2014). Usually, volcanic zircons and apatites can be found in a K-bentonite because these minerals are persistent during the above geological processes. As the deposition of a volcanic ash bed is transient, a K-bentonite is widely used as an isochronous marker bed for stratigraphic correlation (Su et al., 2003; Su et al., 2010; Zhou et al., 2008; Zhou et. al., 2013; Wang et al., 2020a, Wang et al., 2020b). So far, as to the Marinoan cap dolostones around the world, K-bentonites have been found only in the Doushantuo cap dolostone on the Yangtze Platform in South China (Condon et al., 2005; Wan et al., 2013; Xing et al., 2018). Intensive studies have focused on the zircon U-Pb geochronology of the K-bentonites (Condon et al., 2005; Yin et al., 2005; Xing et al., 2018). However, only sporadic work has been conducted on the whole-rock geochemistry of the K-bentonites in the Doushantuo cap dolostones from the platform and slope of the Yangtze Platform, to preliminarily understand the genesis of the K-bentonites (Wan et al., 2013). A study of the whole-rock geochemistry of the K-bentonite found in the Doushantuo cap dolostone from the basin and further on zircon geochemistry

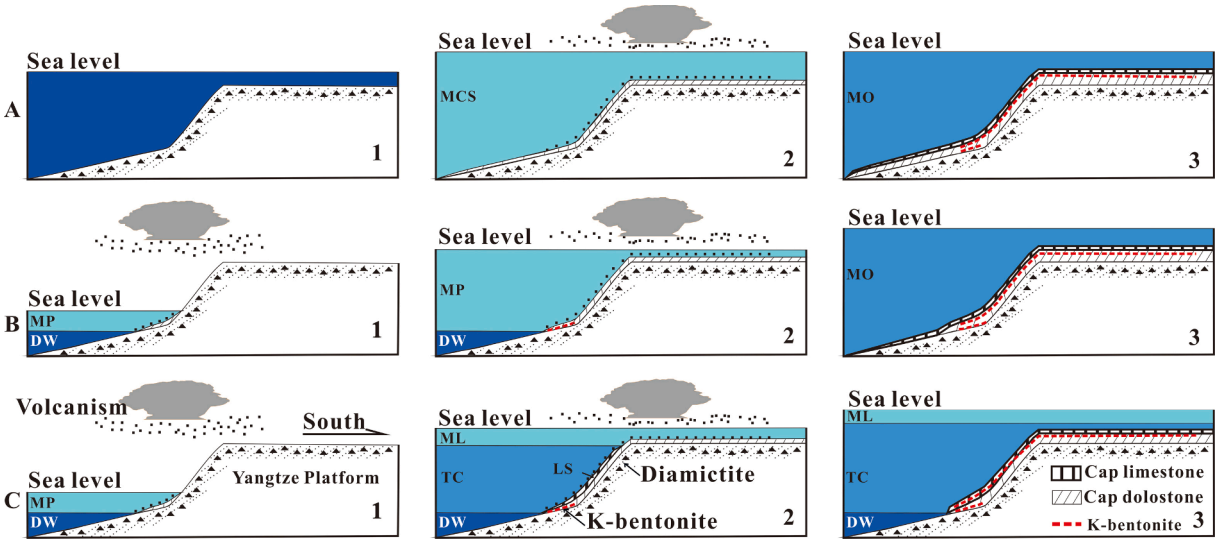

Fig. 1. A supposed distribution model for the K-bentonites in the Doushantuo cap dolostones in South China based on the genetic hypothesis for Marinoan cap carbonates by Hoffman et al. (2007). A: Isochronous model: 1—depth-distance section during glacioeustatic rise, no carbonate deposited; 2—cap dolostone deposited, according to Kennedy et al. (2001), Jiang et al. (2003) and Jiang et al. (2006) in response to methane cold seepage (MCS); within this interval, an early episode of small-scale volcanism would have caused K-bentonites preserved in cap dolostone in deep-water realm, while a late episode of large-scale volcanism may have resulted in K-bentonites occurred in cap dolostones in both deep- and shallow-water areas; 3—cap limestone deposited in response to change in ocean chemistry (MO, mixed ocean). B: Semi-diachronous model: 1—cap dolostone deposited from incipient meltwater plume (MP) above deep water (DW); during this interval, an early episode of volcanism may have led to K-bentonite intercalated in cap dolostone in deep-water region (e.g. the Heyu K-bentonite); 2—meltwater plume grows and floods the bank, cap dolostone deposited diachronously; in this interval, a late episode of volcanism might have resulted in K-bentonite sandwiched in cap dolostone in both deep- and shallow-water realms; 3—limestone deposited, according to Sheilds (2005) in response to mixing of MP and DW. C: Diachronous model: 1—same as B1; 2—meltwater plume differentiates a mixed layer (ML), which deposits cap dolostone, and a thermocline (TC), which simultaneously deposits limestone (LS); during this interval, a late episode of volcanism would have caused K-bentonite preserved in cap dolostone in shallow- and deeper-water regions (e.g. the Jiuqunao and Lantian K-bentonites), and in limestone in deep-water area; 3—TC floods the platform, causing diachronous change from dolostone to limestone at the ML–TC interface.

of the K-bentonites from the entire Yangtze Platform has not been carried out. Consequently, more information concealed in these K-bentonites which may cast light on the relationship between the sedimentary sequences of the cap dolostones and the distribution of the K-bentonites has not been fully unraveled. The purpose of this study is to conduct a more systematic work on the whole-rock and zircon geochemistry of the K-bentonites in the Doushantuo cap dolostones on the Yangtze Platform, in order to reveal the nature of the primary magma, the tectonic setting of the source volcanoes, the possible location of the magma source of the K-bentonites, and to further distinguish the episodes of the source volcanic activities of the K-bentonites. In addition, based on the detailed genetic information of the K-bentonites, we tentatively discuss the possible link between the distribution characteristics of the K-bentonites and the sedimentary model of the cap dolostones.

2. Geological settings

The South China block formed from amalgamation (ca. 880 Ma or soon after) of the Yangtze and Cathaysia blocks during assembly of the supercontinent Rodinia (Li et al., 2009). Subsequently, the separation of the South China block from Rodinia led to the formation of rift basins that were filled with Tonian volcaniclastics, Cryogenian glacial diamictite and interglacial siliciclastic, and Ediacaran siliciclastic and carbonate rocks (Wang and Li, 2003). The Cryogenian glacial deposits occur widely on the Yangtze block in South China, and they are thicker and more complete in the slope and basinal facies from the northern and southeastern margins of the block (Zhou et al., 2004; Zhou et al., 2010; Zhou et al., 2019). For example, three diamictite intervals (the Changan, Tiesiao, and Nantuo diamictites) can be recognized in slope and basinal facies from the southeastern margins, while the Changan and Tiesiao diamictites are missing in platform facies (Zhou et al., 2004). Among the three diamictites, the youngest and widespread Nantuo diamictite has a thickness of more than 1000 m in the northern and southeastern margins, whereas it is generally<500 m in the shallow-water realms (Zhou et al., 2010). The Nantuo diamictite is considered to be equivalent to the Marinoan diamictite elsewhere (Zhou et al., 2004; Jiang et al., 2006; Hoffman et al., 2007). A widespread horizon of dolostone, namely the Doushantuo cap dolostone, overlies the Nantuo diamictite. K-bentonites have been discovered in the Doushantuo cap dolostone during the past two decades (Condon et al., 2005; Wan et al., 2013; Xing et al., 2018).

The Jiuqunao section (30°54′2.1″N, 110°52′64″E) is located in the Three Gorges area in South China, and palaeogeographically in the platform interior of the Yangtze Platform during the Cryogenian-Ediacaran transition (Fig. 2). The oldest stratigraphic unit at this section is the diamictite of the topmost Nantuo Formation. Upwardly, a ca. 4.8 m thick Doushantuo cap dolostone occurs. Approximately 3.8 m above the base of the Doushantuo cap dolostone, a ca. 40 cm thick yellowish brown K-bentonite has been recognized (Fig. 3A, E). The K-bentonite is well correlatable with the K-bentonites discovered in the Doushantuo cap dolostones at the adjacent Huajipo and Jiulongwan sections in the Three Gorges area. Condon et al. (2005) have reported the zircon CA-ID-TIMS U-Pb age (635.2 ± 0.6 Ma) of the K-bentonite at the Huajipo section (Wuhe-Gaojiaxi section).

The Heyu section (31°51′43.4″N, 108°56′54.3″E) is located in the Chengkou area of Chongqing City in South China (Fig. 2), and palaeogeographically in the basin along the northern margin of the Yangtze Platform during the Cryogenian-Ediacaran transition (Zhang et al., 1996; Zhou et al., 2010; Wang et al., 2014; Song et al., 2017; Xing et al., 2018). The oldest stratigraphic unit at this section is the terminal Cryogenian diamictite of the topmost Muzuo Formation. Upwardly, a ca. 3.7 m thick cap dolostone occurs. About 0.7 m above the base of the cap dolostone, a ca. 10 cm thick greenish gray K-bentonite has been discovered (Fig. 3B, F). Xing et al. (2018) obtained an age of 634.1 ± 1.9 Ma for the K-bentonite through a SIMS U-Pb dating carried out on its zircons.

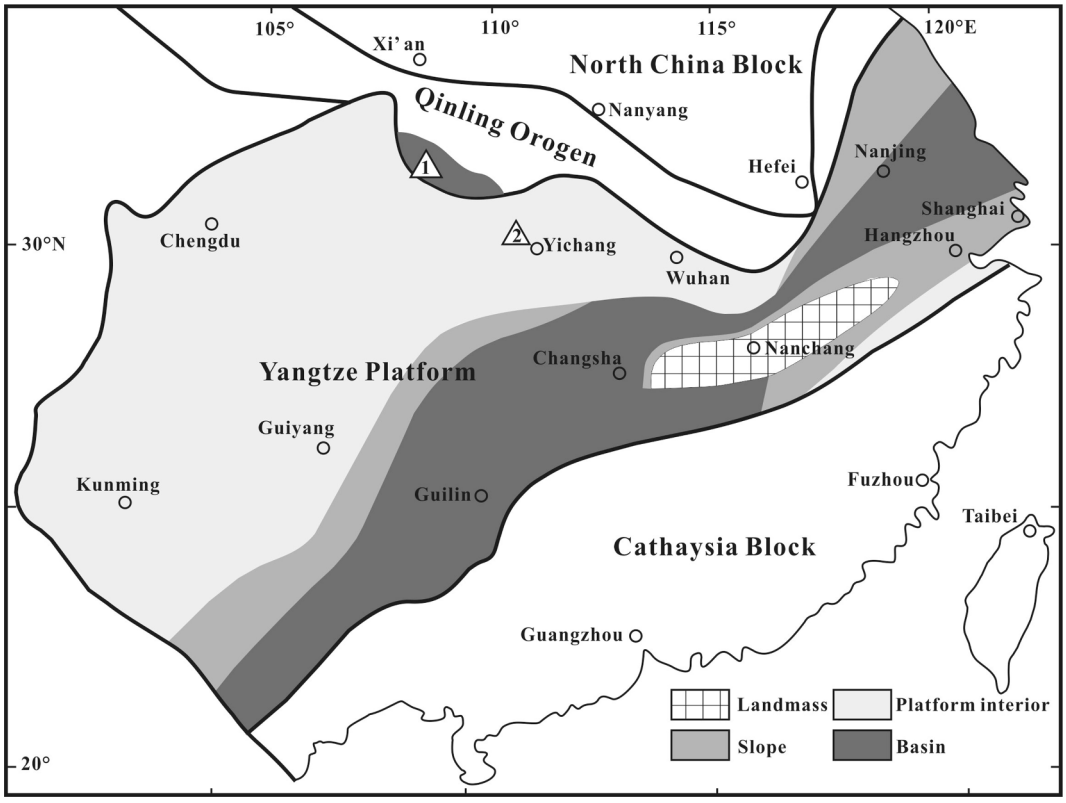

Fig. 2. Ediacaran paleogeography of the Yangtze Block (modified from Zhang et al., 1996; Zhou et al., 2010; Wang et al., 2014; Song et al., 2017; Xing et al., 2018). Numbered triangles indicate locations of Ediacaran sections mentioned in the text. 1—Heyu section; 2—Jiuqunao section.

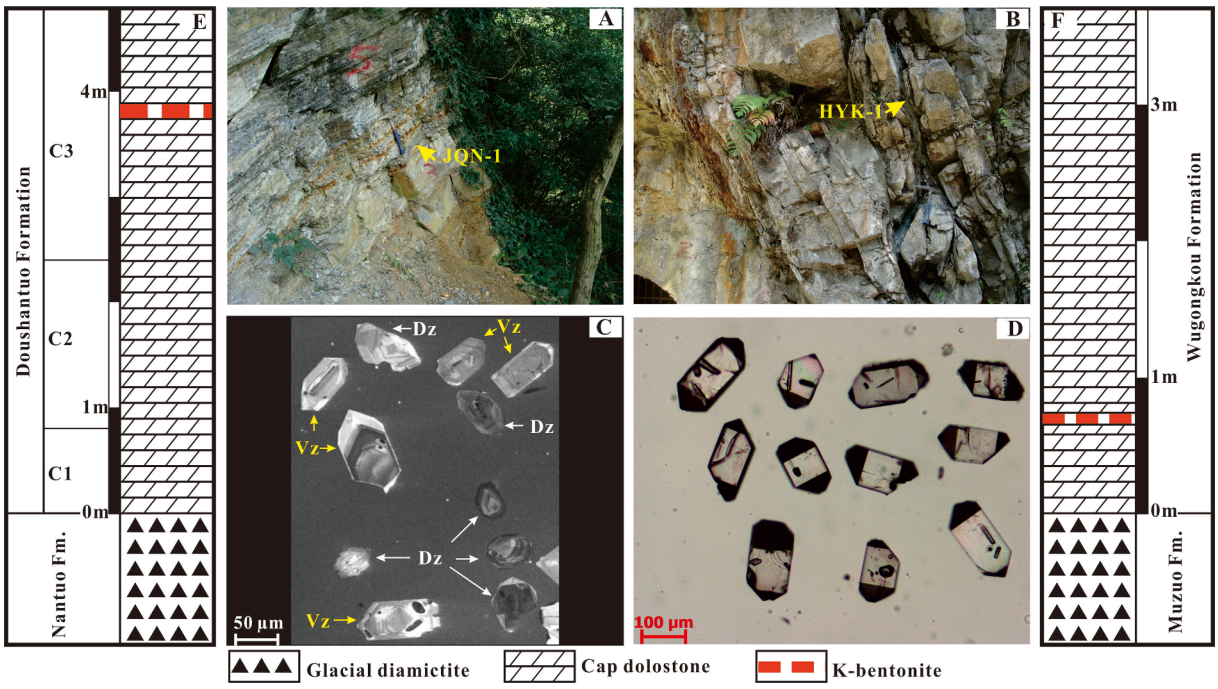

Fig. 3. Field photos of K-bentonites in Doushantuo cap dolostones in South China, photomicrographs of zircons in the K-bentonites, and stratigraphic profiles of the Doushantuo cap dolostones at the Jiuqunao and Heyu sections. A: A yellowish green K-bentonite sandwiched in cap carbonates at Jiuqunao; B: A greenish gray K-bentonite intercalated with the cap dolostones at Heyu; C: Euhedral and rounded zircons (cathodoluminescence image) from the K-bentonite at Jiuqunao; Vz—Volcanic zircon; Dz—Detrital zircon; D: Euhedral zircons (transmitted light photomicrograph) in the K-bentonite at Heyu; E: Stratigraphic profile of the Doushantuo cap dolostone at the Jiuqunao section; Classification of C1 to C3 of the dolostone is after Jiang et al. (2006); F: Stratigraphic profile of the Doushantuo cap dolostone at the Heyu section. The length of the hammer handle in A and B is 30 cm.

3. Sampling and analytical techniques

We collected one sample (labeled JQN-1) of the same K-bentonite within the top of the cap dolostone (ca. 3.8 m above the base of the cap dolostone; Fig. 3A, E) studied by Wan et al. (2013) from the Jiuqunao section. In the study of Wan et al. (2013), the sample number is YCW-01. Meanwhile, we collected one sample (labeled HYK-1) of the K-bentonite within the base of the cap dolostone (0.7 m above the base of the cap dolostone; Fig. 3B, F) studied by Xing et al. (2018) at the Heyu section. As the K-bentonites are relatively soft and loose, the surface layer of the outcrop is susceptible to weathering and contamination by detrital materials. To avoid such problems, digging works were carried out to collect fresh K-bentonites at the Jiuqunao and Heyu sections. A total of 20 kg of each fresh K-bentonite sample was collected. Since Wan et al. (2013) have analyzed the whole-rock major and trace element contents in three sub-samples of their K-bentonite sample from the Jiuqunao section, the present study did not repeat this work. In this study, clay minerals in the K-bentonite samples from the Jiuqunao and Heyu sections were analyzed using XRD, and the whole-rock major and trace element contents of the sample at the Heyu section were analyzed by XRF and ICP-MS, respectively. Zircon grains were extracted from concentrates of each sample processed by conventional magnetic and density techniques. U-Pb age and trace element content of the zircons were analyzed using LA-ICP-MS, and the Hf isotopic compositions of them were analyzed by LA-MC-ICP-MS.

X-ray powder diffraction (XRD) analyses were performed at the Shale Gas Evaluation and Exploitation Key Laboratory of Sichuan Province, Chengdu, China. For powder diffraction analysis the sample was mixed with water to form a suspension and then allowed to settle for thirty minutes in order to isolate the clay-size material. The suspension was dewatered in a centrifuge and the resulting paste smeared in a thin film on a standard petrographic glass slide and allowed to dry. The smear method allows the maximum diffraction effects from the preferred orientation of layer silicates such as clay and mica. Duplicate slides were prepared and treated both with ethylene glycol and heating to 450–550°C, to test for swelling clays (Moore and Reynolds, 1997). Powder diffraction X-ray scans were made over the range of 5-45° 2θ using copper Kα radiation in an X'Pert powder diffractometer. The XRD data were processed using HighScore software. Minerals were identified on the basis of peak position and peak intensity. On each plot the individual peaks are labeled in angstroms (Å) indicating the actual interatomic distance represented by that reflection. When the clay minerals include illite, kaolinite, chlorite and mixed-layer illite–smectite, the percentages of the individual clay minerals were calculated according to following formulas: (1) $K + C = [I_{0.7nm}(\text{Air})/1.5]/[I_{0.7nm}(\text{Air})/1.5 + I_{1.0nm}(\text{Heat})] \times 100\%$, (2) $K = h_{0.358nm}(\text{EG})/[h_{0.358nm}(\text{EG}) + h_{0.353nm}(\text{EG})] \times (K + C)$, (3) $C = (K + C) - K$, (4) $I = \{[I_{1.0nm}(\text{EG}) \times (h_{0.7nm}(\text{Air})/h_{0.7nm}(\text{EG}))]/I_{1.0nm}(\text{Heat})\} \times [100\% - (K + C)]$, and (5) $I/S = 100\% - (I + K + C)$. K, C, I and I/S in the above formulas denote the percentages of kaolinite, chlorite, illite and mixed-layer illite–smectite, respectively. $I_{0.7nm}(\text{Air})$ denotes the peak intensity of 0.700 nm in the plot of the air-dried slide; $I_{1.0nm}(\text{Heat})$ denotes the peak intensity of 1.000 nm in the plot of the slide heating to 450–550°C; $I_{1.0nm}(\text{EG})$ denotes the peak intensity of 1.000 nm in the plot of the slide treated with ethylene glycol; $h_{0.7nm}(\text{Air})$ denotes the height of the peak of 0.700 nm in the plot of the air-dried slide; $h_{0.358nm}(\text{EG})$, $h_{0.353nm}(\text{EG})$ and $h_{0.7nm}(\text{EG})$ denote the heights of the peaks of 0.358 nm, 0.353 nm and 0.700 nm in the plot of the slide treated with ethylene glycol, respectively. The percentage of illite in mixed-layer illite–smectite was calculated according to the following formula: $I/(I/S) = I_{1.0nm}(\text{EG})/[I_{1.0nm}(\text{Heat}) - I_{1.0nm}(\text{EG})]$. $I/(I/S)$ in the formula means the percentage of illite in mixed-layer illite–smectite; $I_{1.0nm}(\text{EG})$ and $I_{1.0nm}(\text{Heat})$ denote the peak intensities of 1.000 nm in the plots of the slides treated with ethylene glycol and heating to 450–550°C, respectively. Whole-rock element concentrations of the K-bentonite were analyzed at the State Key Laboratory of Ore Deposit Geochemistry (SKLODG), Institute of Geochemistry, Chinese Academy of Sciences in Guiyang, China. Major elements in the K-bentonite were determined by an Axios (PW4400) X-

ray fluorescence (XRF) spectrometer. 200 mesh whole-rock powders were admixed with $LiBO_4$ and fused into glass discs at temperature higher than 1025 °C. The discs were then analyzed by the XRF spectrometer. Basaltic to granitic rock standards (NCSDC73303, SARM-2, SARM-3, and SARM-4) were analyzed to monitor the analytical quality, the results of which indicate the uncertainties are within 0.1–1% (RSD). For trace element analyses, 50 mg of powdered K-bentonite sample were placed in a PTFE screw-top bomb. To the sample was added 1 ml of distilled HF and 1 ml of distilled HNO_3. The sealed bomb was then placed in an electric oven and heated to 190 °C for 24 h. After cooling, the bomb was opened and placed on a hot plate, and the solution evaporated to dryness and followed by an addition of 1 ml distilled HNO_3 and evaporation to dryness. Two milliliters of distilled HNO_3 and 3 ml distilled de-ionized water were added. One milliliter of 500 ng/ml Rh solution was added as an internal standard. The resealed bombs were then placed in an electric oven and heated to 140 °C for 5 h. After cooling, 0.4 ml of the solution was transferred to a centrifuge tube, and was made up to a 10 ml by addition of distilled de-ionized water. The solution sample was atomized by a nebulizer, and the sample aerosol was introduced into ICP through a spray chamber. The solution uptake rate was 0.33 ± 0.02 ml/min. Trace element abundances were determined using a PerkinElmer ELAN DRC-e ICP-MS. Duplicate samples were used to estimate the analytical precision. The results show that the relative standard deviations (RSD) of the elements are better than 10%. Accuracy is better than 5% for most of the elements as evaluated from rock standards (OU-6, AGV-2, AMH-1, GBPG-1).

U-Pb dating and trace element analyses of zircons in the K-bentonites were conducted synchronously by LA-ICP-MS at SKLODG. Laser sampling was performed using a *GeoLas Pro* 193 nm ArF excimer laser. A laser frequency of 7 Hz and a spot size of 32 μm were applied to all analyses. An Agilent 7900 ICP-MS instrument was used to acquire ion-signal intensities. Helium was applied as a carrier gas which was mixed with Argon via a T-connector before entering the ICP-MS. Each analysis incorporated a background acquisition of approximately 30 s (gas blank) followed by 60 s of data acquisition from the sample. Off-line selection and integration of background and analyte signals, and time-drift correction and quantitative calibration for trace element analyses and U-Pb dating were performed by ICPMSDataCal software (Liu et al., 2008; Liu et al., 2010). Zircon 91,500 was used as an external standard for U-Pb dating, and was analyzed twice every 6–8 analyses (i.e., 2 zircon 91500 + 6–8 samples + 2 zircon 91500). Preferred U-Th-Pb isotopic ratios used for 91,500 are from Wiedenbeck et al. (1995). Uncertainty of preferred values for the external standard 91,500 was propagated to the ultimate results of the samples. Concordia diagrams and weighted mean calculations were made using Isoplot software (Ludwig, 2003). In this study, the $^{206}Pb/^{238}U$, $^{207}Pb/^{235}U$, $^{207}Pb/^{206}Pb$ ages of the zircons are relatively consistent within errors. Therefore, the U-Pb ages do not need to correct the radiogenic Pb loss with a discordant line. Trace element compositions of zircons were calibrated against multiple-reference materials (NIST 610, BHVO-2G, BCR-2G, BIR-1G) combined with Si internal standardization. The NIST 610 and other standard materials were incorporated into the analytical routine according to an arranged sequence (e.g., NIST 610 + BIR-1G + BHVO-2G + BCR-2G + 2 zircon 91500 + zircon Plešovice + 8 samples + NIST 610 + BIR-1G + BHVO-2G + BCR-2G + 2 zircon 91500 + zircon Plešovice). The preferred values of element concentrations for the USGS reference glasses are from the GeoReM database (http://georem.mpch-mainz.gwdg.de/). Samples were calibrated against the multiple standards using a linear calibration approach in which multiple standards define a calibration curve of variable concentration range for each trace element. The calibration was processed by the ICPMSDataCal software which was programmed with Visual Basic language (Liu et al., 2008; Liu et al., 2010).

In situ zircon Hf isotope measurements were subsequently performed on the dated zircons using a Nu Plasma III MC-ICP-MS coupled with a RESOlution S-155 193 nm ArF excimer laser-ablation system, at SKLODG. A spot size of 40 μm with a repetition rate of 10 Hz was applied to all analyses. The detailed analytical procedures, conditions and data acquisition parameters are provided by Tang et al. (2008). For Hf-isotope determinations, isotopes 172 and 175–180 were measured simultaneously in static-collection mode during a single data acquisition. Data were normalized to $^{179}Hf/^{177}Hf = 0.7325$, using an exponential correction for mass bias. Interference of ^{176}Lu on ^{176}Hf was corrected by measuring the intensity of the interference-free ^{175}Lu isotope and using the recommended $^{176}Lu/^{175}Lu = 0.02669$ (De Biévre and Taylor, 1993) to calculate $^{176}Lu/^{177}Hf$. Similarly, the interference of ^{176}Yb on ^{176}Hf was corrected by measuring the interference-free ^{172}Yb isotope and using $^{176}Yb/^{172}Yb = 0.5865$ to calculate $^{176}Yb/^{177}Hf$. The zircon 91,500 standard was used as the reference material. Our analyses yielded a mean $^{176}Hf/^{177}Hf$ ratio of 0.282303 ± 0.000017 (n = 20, 2-sigma) for the standard, which is consistent with the mean $^{176}Hf/^{177}Hf$ ratio of 0.282302 ± 0.000008 (n = 59, 2 S.D.) for the same standard reported by Goolaerts et al. (2004). A ^{176}Lu decay constant of 1.865×10^{-11} $year^{-1}$ (Scherer et al., 2001) was used for Hf-isotope calculations. Initial $^{176}Hf/^{177}Hf$ ratios, expressed as $(^{176}Hf/^{177}Hf)_i$, were calculated back to the time of zircon crystallization. $\varepsilon_{Hf}(t)$ was calculated relative to a present-day chondritic reservoir with $^{176}Hf/^{177}Hf$ of 0.282772 and $^{176}Lu/^{177}Hf$ of 0.0332 (Blichert-Toft and Albarède, 1997). The one-stage model ages (T_{DM}) were calculated using the measured Lu/Hf ratios and the depleted mantle (DM) evolution curve with a present-day $^{176}Hf/^{177}Hf$ of 0.28325 and $^{176}Lu/^{177}Hf$ of 0.0384 (Vervoort and Blichert-Toft, 1999). The two-stage model ages (T_{DM2}) were calculated under the assumption that the protolith of the host rock of a given zircon was derived from the depleted mantle and had the composition of the average continental crust with $^{176}Lu/^{177}Hf$ of 0.015 (Griffin et al., 2002).

4. Results

4.1. Mineralogy

The clay minerals in the K-bentonites in the Doushantuo cap dolostone from the Jiuqunao section (Fig. 4B) are consisted of illite (39%), kaolinite (30%), chlorite (19%) and mixed-layer illite–smectite (12%). The illite in the mixed-layer illite–smectite accounts for 90%. Some zircons separated from this K-bentonite are euhedral prismatic. However, rounded zircons also can be seen in the zircon concentration (Fig. 3C). The mineral composition of the K-bentonite is consistent with that shown by previous observations (Yin et al., 2005; Wan et al., 2013). The clay minerals in the K-bentonite in the cap dolostone of the Heyu section (Fig. 4A) are composed of illite (75%), kaolinite (13%), chlorite (11%), and a small amount of mixed-layer illite–smectite (1%). The illite in the mixed-layer illite–smectite accounts for 95%. Almost all of the zircons separated from this K-bentonite are euhedral prismatic (Fig. 3D).

4.2. Whole-rock geochemistry

4.2.1. Major-element contents in the K-bentonites

The major element content data of the K-bentonites from the Jiuqunao and Heyu sections are presented in Table 1. The averaged content of SiO_2 in the three sub-samples of the K-bentonite from the Jiuqunao section is 61.07 wt%, which is obviously higher than that of the K-bentonite from the Heyu section (44.74 wt%). The averaged contents of TiO_2, Al_2O_3 and MgO in the three sub-samples of the K-bentonite from the Jiuqunao section are significantly lower than those in the K-bentonite from the Heyu section. The K_2O contents in the K-bentonites from the Jiuqunao and Heyu sections are 6.35 wt% and 7.60 wt%, respectively. Both the K-bentonite from the Jiuqunao and that from the Heyu section have relatively low Na_2O contents, the former's Na_2O content is 0.10 wt% and the latter's Na_2O content is 0.12 wt%.

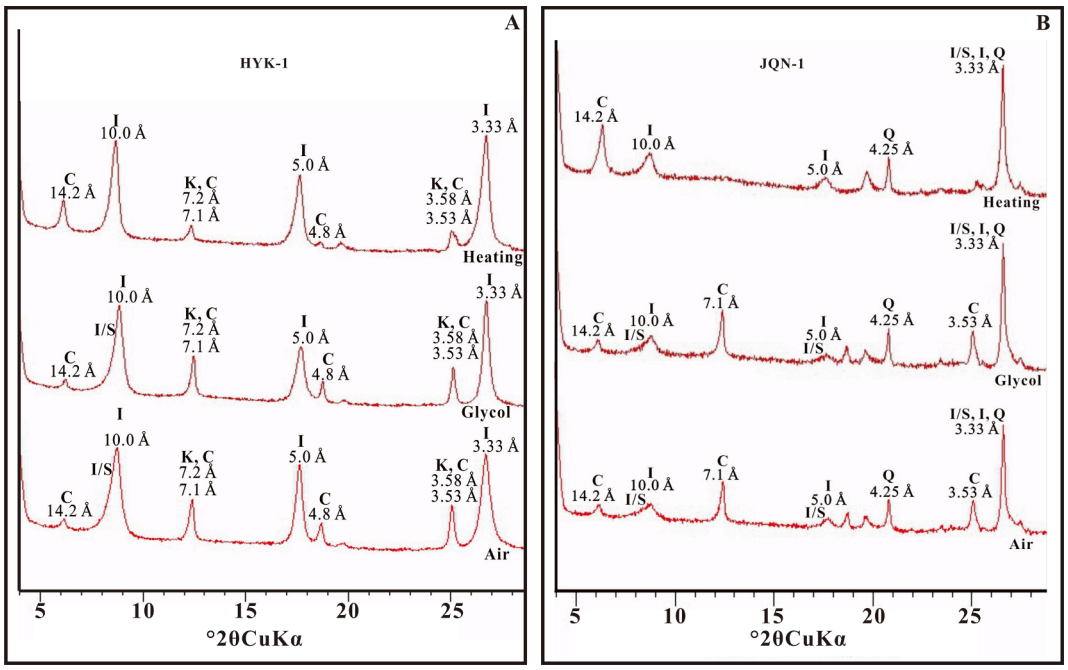

Fig. 4. Powder X-ray diffraction patterns of the clay fraction from the K-bentonites in the Doushantuo cap dolostones at the Heyu (A) and Jiuqunao (B) sections in South China. I, illite; I/S, mixed-layer illite–smectite; K, kaolinite; C, chlorite; Q, quartz.

4.2.2. Trace-element concentrations in the K-bentonites

The trace element concentration data of the K-bentonites from the Jiuqunao and Heyu sections are presented in Table 1. Except for Rb, the Y, Zr, Nb, Hf, Ta, Th, and REE concentrations in the K-bentonite from the Jiuqunao section are significantly lower than those in the K-bentonite from the Heyu section. It is worth noting that the concentrations of Zr, REE and Ta in the Heyu K-bentonite are extremely high, and are up to 2990 ppm, 552 ppm and 16.6 ppm, respectively. K-bentonites from the two sections have typical K-bentonite REE distribution pattern with enriched light rare earth elements, negative Eu anomaly and without obvious Ce anomaly (Zhou et al., 2013; Zhou et al., 2014). Nevertheless, the REE distribution patterns of the K-bentonites from the Jiuqunao and Heyu sections are still significantly different (Fig. 5). The Heyu K-bentonite has more obvious negative Eu anomaly. In addition, the distribution curve of heavy rare earth elements of the Jiuqunao K-bentonite is relatively horizontal, while that of the Heyu K-bentonite is slightly left-dipped.

4.3. Zircon geochronology and geochemistry

4.3.1. Zircon U-Pb ages

The U-Pb age data of zircons in the K-bentonites from the Jiuqunao and Heyu sections are listed in Table 2. We performed LA-ICP-MS U-Pb dating on 21 zircon grains in the K-bentonite from the Jiuqunao section. Among the 21 analysed zircons, 10 zircon U-Pb ages were<90% concordant thus we excluded them from our discussion on their genetic information using their trace element contents and Hf isotopic compositions in this study. In the remaining 11 zircons whose concordances of U-Pb age data are not<90%, 2 zircons (JQN-1–15, JQN-1–20) of them have $^{206}Pb/^{238}U$ ages significantly older than the main population. Considering their rounded crystal, we think that the 2 zircons have a detrital origin. The other 9 zircons have $^{206}Pb/^{238}U$ ages ranging from 595 ± 24 Ma to 633 ± 18 Ma, which are similar to the CA-ID-TIMS $^{206}Pb/^{238}U$ ages (from 611.59 ± 1.04 Ma to 637.11 ± 2.08 Ma) of 12 volcanic zircons in the equivalent K-bentonite from the Huajipo section (Wuhe-Gaojiaxi section) in the Three Gorges area (Condon et al., 2005). Their U-Pb age evidences and euhedral prismatic crystals revealed by their cathodoluminescence (Fig. 3C) and transmitted light images suggest the volcanic origin of these 9 zircons (Chu et al., 2016; Zhou et al., 2018; Yin et al., 2019). Meanwhile, we carried out LA-ICP-MS U-Pb dating on 28 zircons in the K-bentonite from the Heyu section. The concordances of the U-Pb age data of the 28 zircons are higher than 90%. The $^{206}Pb/^{238}U$ age of spot HYK-1–18 is 678 ± 17 Ma and is obviously older than the main population. The zircon hosting the spot is a euhedral crystal. We consider that the zircon is inherited. The other 27 grains are euhedral, and their $^{206}Pb/^{238}U$ age range from 591 ± 56 Ma to 654 ± 23 Ma, which is consistent with the $^{206}Pb/^{238}U$ ages (623.1 ± 9.2 Ma to 643.7 ± 9.2 Ma) of 20 valid spots obtained by Xing et al. (2018) using SIMS method. We believe that the 27 zircons are volcanic.

4.3.2. Zircon trace elements

The in-situ trace element content data of the volcanic zircons in the K-bentonites from the Jiuqunao and Heyu sections are presented in Table 2 and Table 3. For the zircons in the Jiuquao K-bentonite, the Sc concentrations range from 102 to 137 ppm, the Y concentrations range from 1427 to 4010 ppm, the Nb concentrations range from 2.92 to 13.7 ppm, the Hf concentrations range from 6356 to 8397 ppm, the Ta concentrations range from 0.91 to 2.91 ppm, the ΣREE range from 914 to 2561 ppm, the Th concentrations range from 55.2 to 413 ppm, the U concentrations range from 77.2 to 296 ppm, the Th/U ratios range from 0.72 to 1.40. For the zircons in the Heyu K-bentonite, the Sc contents range from 87.5 to 112 ppm, the Y contents range from 2255 to 6312 ppm, the Nb contents range from 20.8 to 64.5 ppm, the Hf contents range from 5759 to 7005 ppm, the Ta contents range from 3.70 to 13.6 ppm, the ΣREE range from 1433 to 4032 ppm, the Th contents range from 84.9 to 618 ppm, the U contents range from 115 to 351 ppm, the Th/U ratios range from 0.74 to 1.76.

The REE distribution patterns of the volcanic zircons in the K-bentonites from the two sections are characterized by depleted light rare earth elements, enriched heavy rare earth elements, obvious positive Ce anomalies and negative Eu anomalies (Fig. 6). We also notice that several volcanic zircons in the K-bentonites from the two sections have flat light rare earth element distribution curves. Although the distribution characteristics of trace elements in the volcanic zircons in K-bentonites from the two sections are generally similar, there are differences in the contents of trace elements such as Sc, Yb, Nb, and Ta. Compared

Table 1
Whole-rock major-element and trace-element compositions of K-bentonites in Doushantuo cap dolostones in South China.

Section	Jiuqunao			Heyu
Sample	YCW-01–1	YCW-01–2	YCW-01–3	HYK-1
(wt%)				
SiO_2	62.28	61.40	59.53	44.74
TiO_2	0.64	0.65	0.60	1.33
Al_2O_3	16.38	16.50	16.40	27.47
Fe_2O_3	2.57	2.66	3.37	3.26
MnO	<0.01	<0.01	<0.01	0.07
MgO	2.49	2.49	2.52	4.00
CaO	<0.01	0.01	<0.01	2.62
K_2O	6.30	6.41	6.34	7.60
Na_2O	0.11	0.10	0.08	0.12
P_2O_5	0.03	0.02	0.03	0.08
LOI	8.08	8.33	8.92	7.95
(ppm)				
Rb	176	177	171	149
Y	41.4	43.4	39.4	238
Zr	234	242	225	2990
Nb	18.0	18.9	17.2	229
Hf	5.70	5.60	5.40	68.3
Ta	1.40	1.30	1.30	16.6
Th	16.5	15.4	16.3	41.4
La	32.8	31.2	31.1	89.8
Ce	53.2	50.7	50.1	204
Pr	5.15	4.97	4.88	20.8
Nd	16.7	16.5	15.6	75.7
Sm	2.86	2.79	2.76	9.62
Eu	0.480	0.480	0.480	1.14
Gd	2.45	2.42	2.32	14.2
Tb	0.460	0.450	0.430	4.15
Dy	3.43	3.29	3.22	39.0
Ho	0.760	0.730	0.720	9.80
Er	2.57	2.50	2.41	35.5
Tm	0.410	0.390	0.390	5.44
Yb	2.76	2.65	2.66	37.3
Lu	0.410	0.380	0.380	5.61
∑REE	124	119	117	552
$(La/Yb)_N$	8.07	8.00	7.94	1.64
Ce/Ce*	0.90	0.89	0.89	1.10
Eu/Eu*	0.54	0.55	0.56	0.30

Note: Data of the K-bentonite at Jiuqunao are those from three sub-samples reported by Wan et al. (2013). Chondrite normalizing values used in the table are after McDonough and Sun (1995). The formulas for calculating Ce/Ce* and Eu/Eu* are: $Ce/Ce^* = 2Ce_N/(La_N + Pr_N)$, $Eu/Eu^* = 2Eu_N/(Sm_N + Gd_N)$. The subscript N in the formulas and table means chondrite-normalized.

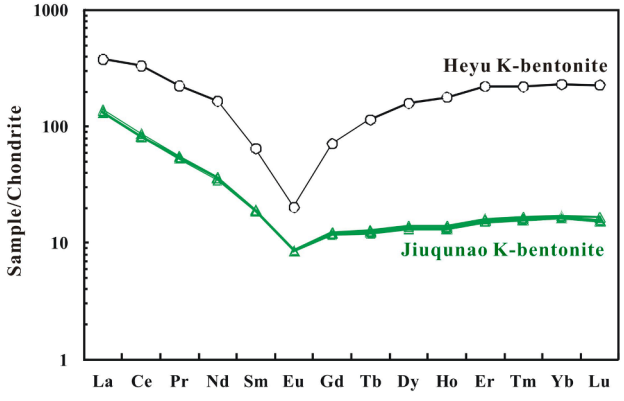

Fig. 5. Chondrite-normalized REE patterns for K-bentonites in the Doushantuo cap dolostone from South China. Chondrite normalizing values are from McDonough and Sun (1995).

with the volcanic zircons in the Jiuqunao K-bentonite, those in the Heyu K-bentonite have higher Yb, Nb, Ta contents and lower Sc contents (Fig. 7).

4.3.3. Zircon Hf isotope composition

The Lu-Hf isotope compositions of the volcanic zircons in the K-bentonites from the Jiuqunao and Heyu sections are listed in Table 4. For the volcanic zircons in the Jiuqunao K-bentonite, the $^{176}Hf/^{177}Hf$ ratios range from 0.282390 to 0.282654, the range of $\varepsilon_{Hf}(t)$ calculated at 635 Ma is – 0.2 ~ 8.5 (with an average of 5.9 ± 0.5), the depleted mantle one-stage model ages (T_{DM1}) range from 882 Ma to 1240 Ma (with an average of 1007 ± 21 Ma), and the depleted mantle two-stage model ages (T_{DM2}) range from 1032 Ma to 1583 Ma (with an average of 1194 ± 32 Ma). For the volcanic zircons in the Heyu K-bentonite, the $^{176}Hf/^{177}Hf$ ratios range from 0.282369 to 0.282656, the range of $\varepsilon_{Hf}(t)$ calculated at 635 Ma is – 0.4 ~ 8.0 (with an average of 5.6 ± 0.4), the depleted mantle one-stage model ages (T_{DM1}) range from 930 Ma to 1223 Ma (with an average of 1021 ± 17 Ma), and the depleted mantle two-stage model ages (T_{DM2}) range from 1067 Ma to 1592 Ma (with an average of 1216 ± 26 Ma).

5. Discussions

5.1. Confirmation the lithology of the K-bentonites

In the present study, we identified the clay rocks preserved in the Doushantuo cap dolostones from the Jiuqunao and Heyu sections as K-bentonites, which is mainly based on the following reasons: (1) The clay minerals in the clay rocks from the two sections are composed of illite, mixed-layer illite–smectite, kaolinite, chlorite and so on, which are typical in K-bentonite (Su et al., 2003; Su et al., 2010; Zhou et al., 2014; Huff, 2016; Zhou et al., 2018). (2) The K_2O contents of the K-bentonites from the Jiuqunao and Heyu sections are 6.35 wt% and 7.60 wt%, respectively, which are similar to those of typical K-bentonites (Zhou et al., 2013; Zhou et al. 2014). (3) The euhedral prismatic zircons in the clay rocks from the two sections have oscillatory and sectoral zoning of magmatic zircons. Besides, they have typical trace-element distribution characteristics of magmatic zircons. Their Th/U ratios are higher than 0.1 (Table 2), and their steep left-inclined chondrite-normalized REE patterns show significant positive Ce anomalies and negative Eu anomalies (Table 3; Fig. 6). It is worth noting that some of these zircons have significantly higher concentrations of light rare earth elements (LREE). Usually, metamictisation of zircons could increase their LREE concentrations. Inclusions in zircons may also cause the enrichment of their LREE. Transmitted light images of these zircons with higher LREE concentrations show that they do contain inclusions, and that they do not have obvious cracks caused by metamictisation (e.g. Fig. 4e, f in Zhou et al., 2018). Zircon U-Pb dating results of these zircons show that they do not have ages significantly younger than the main population, which are resulted from metamictisation (e.g. Fig. 4e, f in Zhou et al., 2018). Therefore, we believe that the higher LREE concentrations of these zircons are caused by the inclusions. Plots of chondrite-normalized LREE/HREE ratios *versus* P, Sc, Y, Nb, Ta, Hf, Th and U concentrations for the volcanic zircons show that except for the P concentrations (with weak positive correlation), the other element concentrations are not correlated with the chondrite-normalized LREE/HREE ratios (Figs. 8, 9), which could suggest that the presence of the inclusions have not changed the distribution patterns of most other trace elements in the zircons. Thus, it would not affect our following genetic interpretations for the K-bentonites based on other trace element concentrations of these zircons.

5.2. Nature of the primary magmas of the K-bentonites

K-bentonite is formed from tuffaceous material that has suffered a series of geological processes. Hence, the information of the nature of its primary magma can not be obtained directly from its whole-rock SiO_2 contents. However, immobile trace elements have been used by numerous workers to provide information on the nature of the primary magma of K-bentonite (Huff et al. 2000; Su et al. 2009; Zhou et al., 2014;

Table 2
LA-ICP-MS U-Pb analyses for zircons in K-bentonites in the Doushantuo cap dolostone from South China.

Sample	Spot	Th	U	Th/U	Atomic ratio						Age		Concordance
		(ppm)			$^{207}Pb/^{206}Pb$	1σ	$^{207}Pb/^{235}U$	1σ	$^{206}Pb/^{238}U$	1σ	$^{206}Pb/^{238}U$	1σ	%
JQN-1	8[a]	83.4	99.5	0.84	0.36863	0.02635	11.75189	1.84181	0.18736	0.01540	1107	84	19
	5[a]	71.8	93.2	0.77	0.39250	0.03095	8.99749	1.05159	0.15546	0.00802	931	45	13
	4[a]	123	142	0.86	0.20062	0.01586	3.86426	0.43398	0.13036	0.00457	790	26	31
	14[a]	98.9	129	0.76	0.14785	0.00934	2.36802	0.16571	0.11493	0.00344	701	20	45
	9[a]	46.1	73.0	0.63	0.07448	0.00533	1.07187	0.08023	0.10424	0.00335	639	20	85
	11[a]	431	656	0.66	0.07678	0.00293	1.07933	0.06761	0.09999	0.00440	614	26	81
	7[a]	116	118	0.99	0.06937	0.00718	0.94726	0.09749	0.09900	0.00277	609	16	89
	13[a]	55.7	83.3	0.67	0.08495	0.00754	1.13786	0.09047	0.09844	0.00556	605	33	75
	1[a]	87.9	109	0.81	0.07945	0.00626	1.06535	0.08634	0.09746	0.00246	600	14	79
	3[a]	839	750	1.12	0.07693	0.00470	0.23617	0.01490	0.02240	0.00058	143	4	59
	20[b]	123	686	0.18	0.07598	0.00246	1.77113	0.06538	0.16805	0.00429	1001	24	96
	15[b]	103	136	0.76	0.06477	0.00652	1.12971	0.13100	0.12535	0.00652	761	37	99
	16	55.2	77.2	0.72	0.05972	0.00354	0.84096	0.04768	0.10322	0.00300	633	18	97
	19	90.4	117	0.77	0.06079	0.00482	0.85976	0.06296	0.10233	0.00212	628	12	99
	2	99.2	113	0.88	0.06935	0.00362	0.94535	0.05080	0.09976	0.00282	613	17	90
	21	108	124	0.87	0.06044	0.00356	0.84272	0.05536	0.09978	0.00267	613	16	98
	10	262	206	1.27	0.06090	0.00272	0.82776	0.03659	0.09833	0.00228	605	13	98
	6	413	296	1.40	0.06327	0.00272	0.84641	0.03647	0.09795	0.00316	602	19	96
	17	117	120	0.98	0.06578	0.00590	0.89972	0.09632	0.09790	0.00377	602	22	92
	18	341	287	1.19	0.06395	0.00348	0.87113	0.05745	0.09787	0.00337	602	20	94
	12	124	157	0.79	0.06650	0.00566	0.88872	0.08080	0.09666	0.00409	595	24	91
HYK-1	18[b]	223	236	0.95	0.06087	0.00509	0.93004	0.07426	0.11089	0.00476	678	17	98
	22	564	345	1.63	0.06128	0.00271	0.90357	0.04442	0.10672	0.00392	654	23	99
	14	154	192	0.81	0.05731	0.00317	0.88703	0.04943	0.10623	0.00238	651	14	95
	19	393	287	1.37	0.06082	0.00398	0.88819	0.05575	0.10631	0.00406	651	24	99
	13	101	126	0.81	0.05759	0.00320	0.87574	0.04772	0.10560	0.00256	647	15	95
	15	148	149	0.99	0.05660	0.00333	0.87597	0.04796	0.10491	0.00296	643	17	94
	1	127	140	0.90	0.05700	0.00584	0.84264	0.08216	0.10435	0.00170	640	13	94
	7	214	225	0.95	0.05757	0.01790	0.86517	0.04000	0.10416	0.00155	639	19	95
	8	151	173	0.87	0.06057	0.02096	0.87474	0.04000	0.10406	0.00171	638	20	99
	20	238	203	1.17	0.05898	0.00263	0.86040	0.04896	0.10399	0.00342	638	20	98
	2	237	236	1.01	0.06000	0.00797	0.86046	0.05000	0.10382	0.00709	637	11	98
	23	428	287	1.49	0.05780	0.00228	0.88682	0.03234	0.10369	0.00277	636	16	96
	17	167	159	1.05	0.05990	0.00282	0.86202	0.04445	0.10353	0.00293	635	17	99
	5	149	153	0.98	0.05754	0.01381	0.86880	0.05000	0.10338	0.00120	634	20	95
	21	240	226	1.06	0.05773	0.00261	0.87191	0.03723	0.10343	0.00296	634	17	95
	6	205	181	1.13	0.05515	0.01524	0.87326	0.04000	0.10314	0.00138	633	19	93
	27	399	288	1.38	0.06119	0.00282	0.86708	0.04304	0.10310	0.00377	633	22	99
	24	419	284	1.48	0.05963	0.00271	0.85115	0.04775	0.10302	0.00399	632	23	98
	16	196	177	1.11	0.05842	0.00266	0.83248	0.04242	0.10251	0.00257	629	15	97
	11	327	227	1.44	0.06017	0.00270	0.88323	0.03788	0.10179	0.00242	625	14	99
	25	618	351	1.76	0.06024	0.00270	0.85087	0.04437	0.10189	0.00348	625	20	99
	26	84.9	115	0.74	0.06217	0.00683	0.85889	0.07496	0.10160	0.00409	624	24	99
	28	301	239	1.26	0.05988	0.00235	0.83281	0.03762	0.10027	0.00252	616	15	99
	12	113	139	0.81	0.06071	0.00464	0.88827	0.04000	0.10003	0.00496	615	19	99
	10	250	181	1.39	0.06240	0.00329	0.86367	0.05076	0.09903	0.00225	609	13	96
	3	257	232	1.11	0.05923	0.00996	0.80283	0.13581	0.09772	0.00803	601	47	99
	9	269	200	1.34	0.06559	0.00268	0.88713	0.03758	0.09761	0.00207	600	12	92
	4	169	168	1.00	0.06310	0.01354	0.82847	0.17504	0.09599	0.00958	591	56	96

Note: Sample JQN-1 is from the Jiuqunao section, and sample HYK-1 the Heyu section. [a] indicates spots with U-Pb ages with concordance<90%. [b] denotes spots from detrital (sample JQN-1) and inherited (sample HYK-1) zircons in the K-bentonites.

Hong et al., 2019a, Hong et al., 2019b). TiO_2 and the trace elements Zr, Nb, and Y are commonly considered to be immobile under processes of weathering, diagenesis, and low-grade metamorphism, and are thus useful indicators of past rock history. The Nb/Y ratio is widely used as an index of alkalinity and Zr/TiO_2 as a measure of differentiation. According to the Nb/Y and Zr/TiO_2 ratios of igneous rocks of known origin, Winchester and Floyd (1977) generated a plot of Nb/Y against Zr/TiO_2 that is organized around the petrology of the original rock type. The K-bentonite from the Jiuqunao section is plotted in the field of rhyodacite (dacite), while that from the Heyu section falls into the field of pantellerite (comendite) (Fig. 10). This result preliminarily shows that the K-bentonites from the two sections have different nature of primary magma. Compared with the primary magma of the K-bentonite from the Jiuqunao section, that of the K-bentonite from the Heyu section is more alkaline and evolved. Watson (1979) has proved that pantellerite (comendite) is extremely rich in Zr, REE, and Ta by his experiments. The typical pantellerite from Pantelleria in Italy is actually rich in Zr, REE and Ta (White et al., 2009). Pantellerite and comendite frequently comprise the felsic end-member in bimodal suites in continental rift and oceanic island settings. White et al. (2009) proposed that the evolved pantellerite and comendite magmas should be the result of fractional crystallization of transitional basalt or metaluminous trachyte magmas. Thus, it is resonable that the incompatible elements Zr, REE and Ta are commonly enriched in pantellerite and commendite. Therefore, the extremely high Zr, REE and Ta contents in the K-bentonite from the Heyu section, indicate that Zr, REE and Ta are immobile during the formation of K-bentonites, and that it is feasible to use elements such as REE, Zr and Ta to discuss the nature of the primary magma of K-bentonites and its difference (Zhou et al., 2013; Zhou et al., 2014). Thus, the obviously different REE distribution pattern of the K-bentonites from the Jiuqunao and Heyu sections also supports the above-mentioned conclusion that the K-bentonites from the two sections have different nature of primary magma.

The concentrations of trace elements in volcanic zircons of K-

Table 3
LA-ICP-MS trace element analytical results (ppm) of volcanic zircons in K-bentonites in the Doushantuo cap dolostone from South China.

Sample	Spot	P	Sc	Y	Nb	La	Ce	Pr	Nd	Sm	Eu	Gd	Tb	Dy	Ho	Er	Tm	Yb	Lu	Hf	Ta
JQN-1	2	890	102	1465	3.54	32.5	86.3	10.9	55.3	18.3	1.17	47.5	14.0	160	55.8	222	42.5	355	64.3	6805	1.14
	6	634	107	2307	10.7	11.2	58.2	4.32	23.4	16.7	1.40	73.1	23.4	260	86.2	349	64.1	534	92.7	7075	2.55
	10	545	123	2269	8.04	0.54	33.7	0.52	6.73	10.3	1.10	61.9	19.3	221	79.6	330	63.2	548	97.8	7418	2.26
	12	196	120	1755	4.35	0.14	13.9	0.52	6.82	8.66	1.31	46.6	13.7	167	60.2	246	45.3	384	67.0	7638	1.32
	16	170	109	1431	2.92	0.051	5.37	0.30	5.12	8.85	1.08	43.4	13.2	139	49.6	206	38.8	347	62.3	6356	0.91
	17	280	137	2379	4.27	3.63	19.2	1.56	14.5	15.7	2.33	79.9	21.4	239	81.1	357	64.6	539	98.7	8397	1.03
	18	535	131	4010	13.7	2.15	49.9	1.14	18.2	24.2	1.45	118	36.7	399	138	581	110	923	159	8089	2.91
	19	450	131	1498	5.07	10.0	34.3	3.54	19.1	10.5	0.86	42.7	13.0	139	47.1	208	40.4	372	65.3	7861	1.50
	21	184	119	1427	4.76	0.045	17.7	0.30	5.97	8.94	0.16	39.6	12.1	132	46.3	200	39.4	349	62.3	7845	1.37
HYK-1	1	367	102	2255	27.2	0.005	34.2	0.19	4.26	8.26	0.81	58.6	19.8	233	80.9	326	60.7	520	86.5	6583	6.71
	2	410	98.8	4347	35.5	0.060	44.9	0.42	8.18	18.0	1.73	120	39.5	468	161	615	117	954	153	6044	7.89
	3	435	111	3379	44.7	0.035	55.3	0.26	6.35	12.6	1.28	86.6	29.5	346	122	481	88.8	736	121	6875	10.7
	4	622	107	3417	36.8	30.3	120	10.1	55.4	27.2	2.31	105	32.0	375	127	491	92.4	780	131	6950	7.98
	5	335	112	2438	29.0	0.042	38.3	0.24	4.64	10.3	1.07	59.6	20.8	251	87.7	350	66.6	556	93.9	6979	7.55
	6	455	104	6312	20.8	0.21	42.5	1.34	23.9	43.7	4.93	221	66.0	692	227	920	171	1384	234	5816	3.70
	7	397	105	2941	48.0	0.083	41.6	0.22	4.00	10.2	1.10	70.3	24.4	297	105	419	79.0	645	107	7005	10.8
	8	437	108	3178	37.1	0.028	53.0	0.33	5.99	13.6	1.62	86.9	28.2	334	115	451	84.5	726	122	6644	9.20
	9	481	101	2951	38.2	0.041	50.8	0.32	6.23	13.3	1.57	84.6	29.2	324	114	441	82.1	656	108	6546	9.29
	10	406	96.2	2492	45.0	0.062	39.6	0.37	6.54	11.7	1.53	68.5	22.6	264	95.5	384	68.8	578	94.0	5959	8.17
	11	645	93.6	3017	49.4	0.28	55.4	0.55	7.72	14.7	1.61	83.8	29.9	334	121	465	85.1	687	112	6009	9.51
	12	579	95.0	2643	29.2	5.73	48.2	2.87	10.9	12.5	1.52	75.3	25.2	289	106	410	77.7	641	102	6232	6.87
	13	357	97.0	2350	24.8	5.03	43.4	1.54	10.9	12.4	1.33	69.7	21.8	251	90.4	376	71.3	595	98.2	6401	6.31
	14	404	92.9	2946	45.8	0.26	47.5	0.25	4.33	9.96	1.17	74.5	27.4	326	117	468	82.9	666	109	6437	10.4
	15	322	97.4	2315	25.8	0.14	33.5	0.28	4.98	10.6	1.16	59.7	21.2	242	88.1	364	68.1	525	85.9	6453	6.92
	16	359	96.7	2472	29.5	0.23	39.1	0.73	5.06	11.0	1.14	67.8	23.4	261	95.9	392	70.4	576	98.3	6470	8.22
	17	372	96.8	2664	34.6	0.71	46.4	0.31	5.14	11.9	1.13	71.0	23.8	281	100	406	75.0	605	98.9	6467	8.13
	19	446	91.5	4481	51.0	0.047	71.1	0.57	10.1	19.8	2.14	134	43.2	495	174	650	117	943	151	6147	11.2
	20	527	96.0	2778	37.6	0.008	47.9	0.26	5.96	11.9	1.37	74.4	25.3	289	106	424	77.5	626	102	6603	8.59
	21	399	93.2	3685	36.4	0.051	47.2	0.34	6.88	15.7	1.52	96.3	32.5	377	134	517	93.5	760	130	6279	8.97
	22	498	95.3	4927	64.5	0.033	82.9	0.52	9.71	21.1	2.36	135	44.9	498	179	685	125	975	162	6385	13.6
	23	404	90.4	4114	60.9	0.052	77.7	0.43	7.39	16.4	1.62	107	37.1	425	154	588	105	843	139	6390	12.5
	24	444	88.4	4440	52.2	0.039	67.2	0.37	7.47	17.9	1.86	113	39.0	426	157	608	109	859	144	6460	11.5
	25	462	87.5	4484	63.4	0.068	84.8	0.53	9.05	21.5	2.15	134	42.4	480	167	641	114	924	153	5759	13.4
	26	314	88.1	2440	29.9	0.012	38.1	0.21	5.90	9.81	0.92	57.5	21.1	238	90.2	362	68.6	550	95.5	6488	7.32
	27	568	88.0	4032	52.0	0.017	65.0	0.38	6.37	15.8	1.41	104	36.6	414	150	558	101	807	133	6312	12.1
	28	416	89.9	3482	46.5	0.028	55.4	0.29	6.06	13.3	1.42	89.2	30.6	347	127	493	89.3	738	120	6415	10.8

Note: Sample JQN-1 is from the Jiuqunao section, and sample HYK-1 the Heyu section.

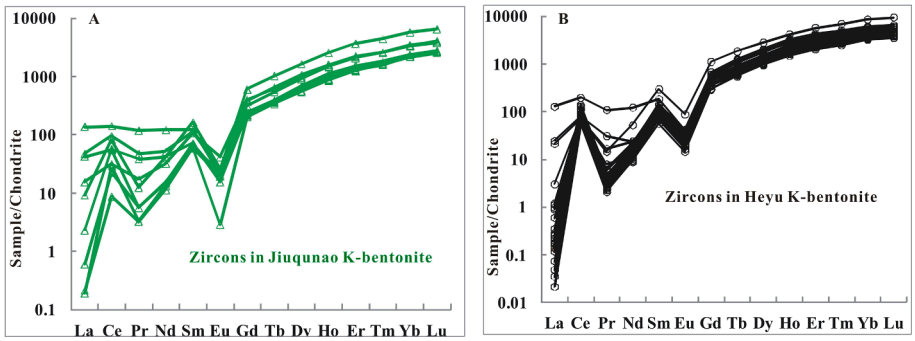

Fig. 6. Chondrite-normalized REE patterns for the volcanic zircons in K-bentonites in the Doushantuo cap dolostone from South China. Chondrite normalizing values are from McDonough and Sun (1995).

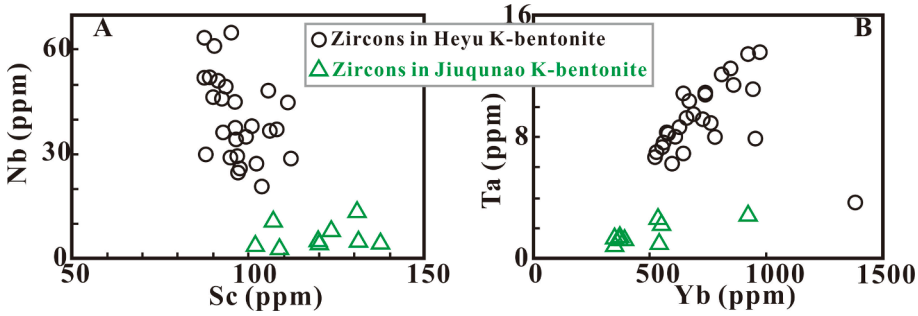

Fig. 7. Scatter plots of Sc *versus* Nb (A) and Yb *versus* Ta (B) for the volcanic zircons from K-bentonites in the Doushantuo cap dolostone in South China, separating the zircons in K-bentonite from different section.

Table 4
LA-MC-ICP-MS Hf isotope compositions of the volcanic zircons in the K-bentonites in the Doushantuo cap dolostones from South China.

Sample	Spot	$^{176}Yb/^{177}Hf$	$^{176}Lu/^{177}Hf$	$^{176}Hf/^{177}Hf$	2σ	$\varepsilon_{Hf}(t)$	2σ	T_{DM1}/Ma	2σ/Ma	T_{DM2}/Ma	2σ/Ma
JQN-1	2	0.048732	0.001617	0.282390	0.000027	−0.2	1.0	1240	38	1583	60
	6	0.184774	0.004362	0.282572	0.000010	5.1	0.4	1057	15	1248	22
	10	0.101041	0.002503	0.282584	0.000013	6.3	0.5	985	19	1171	29
	12	0.017477	0.000666	0.282624	0.000022	8.5	0.8	882	31	1032	49
	16	0.136211	0.003172	0.282582	0.000011	5.9	0.4	1007	16	1194	25
	17	0.168103	0.003898	0.282613	0.000010	6.7	0.4	980	15	1144	22
	18	0.196868	0.004605	0.282654	0.000011	7.9	0.4	937	17	1071	25
	19	0.157682	0.003638	0.282613	0.000013	6.8	0.5	973	20	1137	29
	21	0.192413	0.004491	0.282609	0.000010	6.4	0.4	1004	16	1168	22
HYK-1	1	0.133649	0.003057	0.282576	0.000010	5.8	0.4	1013	15	1205	22
	2	0.184775	0.004363	0.282573	0.000012	5.1	0.4	1056	19	1246	27
	3	0.101051	0.002504	0.282583	0.000015	6.3	0.5	987	22	1174	34
	4	0.185362	0.004332	0.282601	0.000012	6.1	0.4	1012	19	1183	27
	5	0.168104	0.003899	0.282614	0.000011	6.8	0.4	979	17	1141	25
	6	0.156875	0.003713	0.282643	0.000010	7.9	0.4	930	15	1072	22
	7	0.157683	0.003639	0.282614	0.000010	6.9	0.4	972	15	1135	22
	8	0.112426	0.002667	0.282574	0.000013	5.9	0.5	1005	19	1200	29
	9	0.196869	0.004606	0.282656	0.000012	8.0	0.4	934	19	1067	27
	10	0.136212	0.003173	0.282583	0.000010	6.0	0.4	1006	15	1193	22
	11	0.128567	0.002984	0.282547	0.000010	4.8	0.3	1053	15	1267	22
	12	0.144806	0.003346	0.282591	0.000010	6.2	0.4	998	15	1179	22
	13	0.192414	0.004490	0.282610	0.000011	6.4	0.4	1002	17	1166	25
	14	0.169948	0.003946	0.282605	0.000011	6.4	0.4	995	17	1164	25
	15	0.138506	0.003186	0.282583	0.000011	6.0	0.4	1007	16	1193	25
	16	0.099067	0.002454	0.282556	0.000017	5.3	0.6	1026	25	1234	38
	17	0.126909	0.003024	0.282604	0.000011	6.8	0.4	970	16	1141	25
	26	0.121232	0.003207	0.282530	0.000012	4.1	0.4	1085	18	1311	27
	27	0.080183	0.001901	0.282450	0.000011	1.8	0.4	1163	16	1457	25
	28	0.009511	0.000187	0.282369	0.000011	−0.4	0.4	1223	15	1592	24

Note: Sample JQN-1 is from the Jiuqunao section, and sample HYK-1 the Heyu section. Calculation of $\varepsilon_{Hf}(t)$ is based on the precisely estimated age of 635 Ma for the zircons by Condon et al. (2005).

bentonites also can provide information on the nature of the primary magma of K-bentonites (Gao et al., 2013). Most of the zircons in the K-bentonite from the Jiuqunao section fall into the quartz-bearing intermediate and felsic rocks field of the Hf *versus* Y diagram, while the zircons in the K-bentonite from the Heyu section fall into the felsic rocks with 'high' SiO_2 content field of the diagram (Fig. 11A). Both the zircons

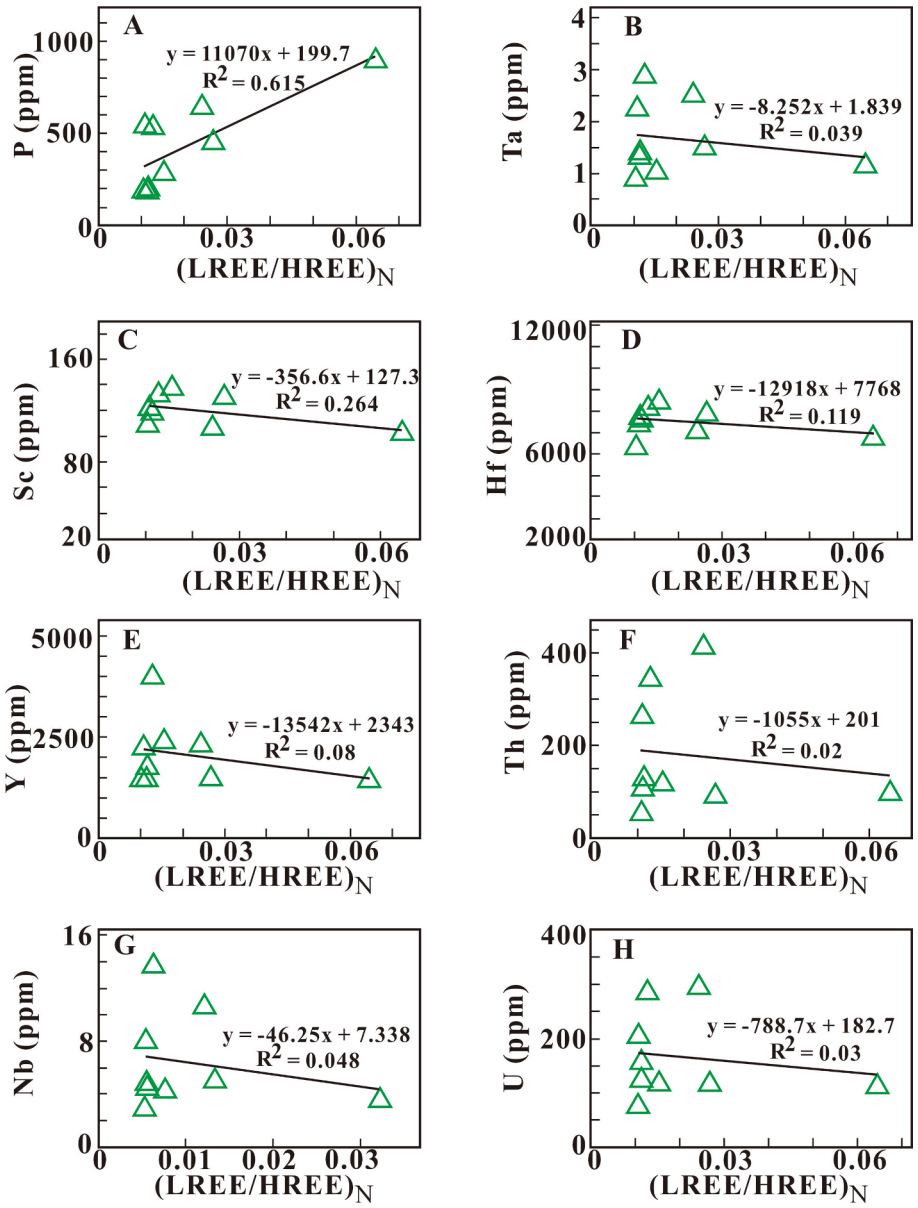

Fig. 8. Plots of chondrite-normalized LREE/HREE ratios *versus* P, Sc, Y, Nb, Ta, Hf, Th and U concentrations for the volcanic zircons of the K-bentonite in the Doushantuo cap dolostone at the Jiuqunao section. Chondrite normalizing values are from McDonough and Sun (1995).

in the K-bentonites from the two sections fall into the hypersolvus alkaline granites/rhyolites field of the Y_2O_3 *versus* HfO_2 diagram (Fig. 11B). These discrimination results suggest that the primary magmas of the K-bentonites from the two sections are felsic in nature. However, the plotted fields of the zircons in the K-bentonites from the two sections do not overlap obviously. Therefore, it is believed that the K-bentonites from the two sections may have different primary magmas (Fig. 11). Compared with the K-bentonite from the Jiuqunao section, the K-bentonite from the Heyu section has more evolved primary magma (Fig. 11A), which is consistent with the information obtained from above whole-rock geochemistry of the K-bentonites.

5.3. Source and tectonic setting of the volcanoes of the K-bentonites

Using the Y-Nb (Fig. 12A) and (Y + Nb)-Rb diagrams (Fig. 12B) based on whole-rock trace element contents, the tectonic settings of source volcanoes of K-bentonites can be preliminarily discriminated (Huff et al. 2000; Su et al. 2009; Zhou et al., 2014; Ge et al., 2019). In the Y-Nb and (Y + Nb)-Rb diagrams, the K-bentonite samples from the Heyu and Jiuqunao sections fall into the within plate granites field (Fig. 12). Through the Hf-U/Yb, Y-U/Yb, Th/U-Nb/Hf and Th/Nb-Hf/Th diagrams based on concentrations of trace elements in zircons, the information on tectonic setting of the source volcano of a K-bentonite can be further obtained (Fig. 13; Grimes et al., 2007; Gao et al., 2013 and references therein; Hawkesworth and Kemp, 2006; Yang et al., 2012). In the Hf-U/Yb (Fig. 13A) and Y-U/Yb diagrams (Fig. 13B), most zircons in the K-bentonites from the Jiuqunao and Heyu sections fall into the field with extensional settings (rift or divergent continental margin) rather than convergent setting. In the Th/U-Nb/Hf (Fig. 13C) and Th/Nb-Hf/Th diagrams (Fig. 13D), all of zircons in the K-bentonite from the Heyu section fall into the within-plate/anorogenic field, part of zircons in the K-bentonite from the Jiuqunao section are plotted into the within-plate/anorogenic field, while some zircons in the K-bentonite at Jiuqunao fall into the field where the within-plate/anorogenic area overlaps with the arc-related/orogenic area. Above results suggest that the tectonic positions of source volcanoes of the K-bentonites from the Heyu and Jiuqunao sections should be located in extensional within-plate settings. Wang and Li (2003) believe that rift basins existed in the western,

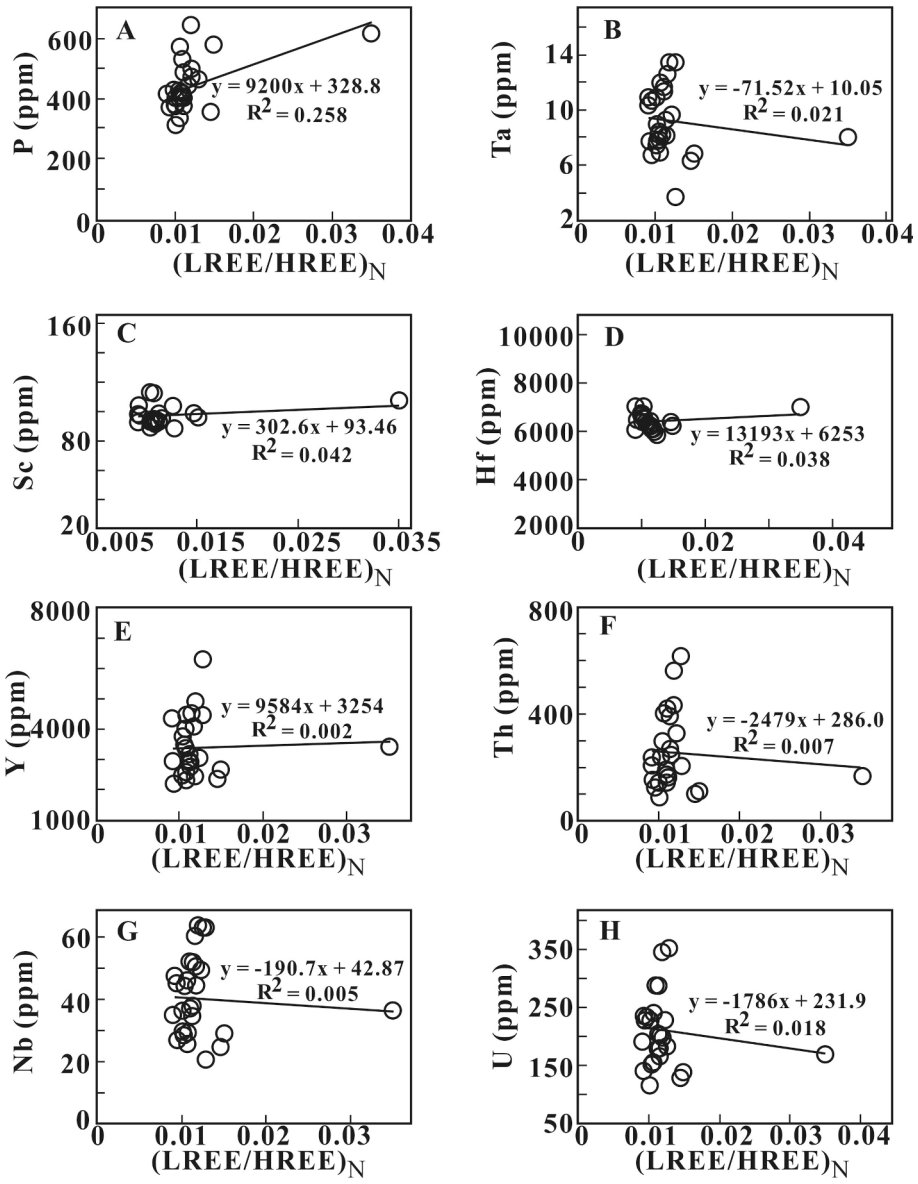

Fig. 9. Plots of chondrite-normalized LREE/HREE ratios *versus* P, Sc, Y, Nb, Ta, Hf, Th and U concentrations for the volcanic zircons of the K-bentonite in the Doushantuo cap dolostone at the Heyu section. Chondrite normalizing values are from McDonough and Sun (1995).

southeastern and northern margins of the Yangtze Block during the Marinoan, but volcanisms from the rift basins of the western and southeastern margins ceased in this age. Some workers (Tao et al., 1985; Zhang et al., 1996) believe that the rift system on the northern margin of the Yangtze Block was still extending in the end-Neoproterozoic, and that volcanic activity from this region still existed during this interval. Therefore, the source volcanoes of the K-bentonites in this study are more likely to occur in the extensional setting on the northern margin of the Yangtze Block (Wang et al., 2020a, Wang et al., 2020b), which agrees well with that the K-bentonites in the Marinoan cap dolostones in South China are mainly found in the sections from the northern margin of the Yangtze Block.

The source information of primary magmas of K-bentonites can be obtained using Hf isotopic compositions and trace element concentrations of zircons in the K-bentonites (Wang and Pupin, 1992; Gao et al., 2013; Guo et al., 2019). The ε_{Hf} (635 Ma) values of 9 volcanic zircons in the K-bentonite from the Jiuqunao section range from − 0.2 to 8.5 (mean = 5.9 ± 0.5), and those of 20 volcanic zircons from the Heyu section range from − 0.4 to 8.0 (mean = 5.6 ± 0.4). In the $\varepsilon_{Hf}(t)$ *versus* age diagram, all zircons in the K-bentonites from the two sections are plotted below the depleted mantle Hf isotope evolution line (Fig. 14). Therefore, it can be interpreted that the primary magmas of the K-bentonites from the two sections are mainly from the mantle, and have an addition of crustal materials. The U, Y, and Th in zircons of K-bentonites from the two sections have positive correlation (Fig. 15A-D), but the Y and P in these zircons are not correlated (Fig. 15E, F), which also indicates that the primary magmas of the K-bentonites are mainly mantle-derived in nature (Wang and Pupin, 1992). The two-stage Hf model ages (T_{DM2}) of zircons in K-bentonites from the Jiuqunao and Heyu sections have ranges of 1032–1583 Ma (mean = 1194 ± 32 Ma) and 1067–1592 Ma (mean = 1216 ± 26 Ma), respectively. These two-stage Hf model ages agree well with the age of crustal accretion event from the northern margin of the Yangtze Block (Ao et al., 2014). Thererore, it suggests that the primary magmas of the K-bentonites may have mixed with the crustal materials from the northern margin of the Yangtze Block.

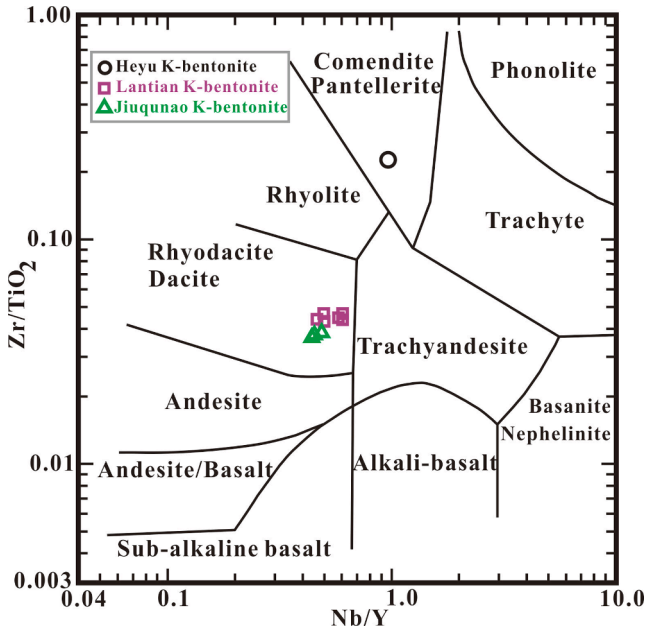

Fig. 10. Nb/Y *versus* Zr/TiO_2 plot (Winchester and Floyd, 1977) of the K-bentonites in the Doushantuo cap dolostone from South China. The data of the Lantian K-bentonite are from Wan et al. (2013).

5.4. Source volcanic episodes of the K-bentonites and their potential significance to the genesis of the Marinoan cap dolostone

The K-bentonites in the Doushantuo cap dolostones from the Heyu and Jiuqunao sections differ in nature of their primary magmas, although their source volcanoes have similar tectonic settings. Therefore, the K-bentonites from the two sections most probably represent the records of volcanic eruptions of two different episodes. The K-bentonite from the Heyu section is within the bottom of the Doushantuo cap dolostone of the section (0.7 m above the base of the cap dolostone), while the K-bentonite from the Jiuqunao section is within the top of the cap dolostone of the section (Fig. 3A, B, E, F). The Heyu and Jiuqunao sections are palaeogeographically located in the basin and platform interior of the Yangtze Platform, respectively (Fig. 2). Hence, whichever model in Fig. 1 the sedimentary sequence of the Marinoan cap dolostones agrees with, the K-bentonite from the Heyu section most probably represents the record of volcanic eruption of the old episode. The geochemical characteristics of the K-bentonite in the Doushantuo cap dolostone from the Jiuqunao section (in platform) are completely similar to those of the K-bentonite in the cap dolostone from the Lantian section (in slope) in the Xiuning area, Anhui Province, South China (Fig. 7; Wan et al., 2013). Consequently, the K-bentonites from the Jiuqunao and Lantian sections should be the records of volcanic eruption in the same episode. To date, the K-bentonite of the old volcanic episode has only been found in the Heyu section in the basinal area, while the K-bentonite from the young volcanic episode has been

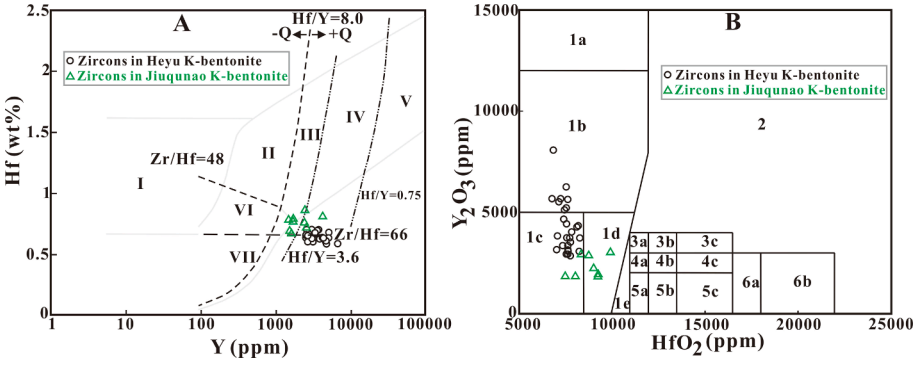

Fig. 11. Trace-element diagrams for the volcanic zircons from the K-bentonites in the Doushantuo cap dolostone in South China, showing discrimination of potential sources. A: Hf *versus* Y (Shnukov et al., 1997; Belousova et al., 2002); B: Y_2O_3 *versus* HfO_2 (Pupin, 2000). In diagram A: I, kimberlites; II, ultramafic, mafic and intermediate rocks; III, quartz-bearing intermediate and felsic rocks; IV, felsic rocks with 'high' SiO_2 content; V, greisens; VI, alkaline rocks and alkaline metasomatites of alkaline complexes; and VII, carbonatites. In diagram B: 1a, tholeiitic plagiogranites; 1b-c-d-e, hypersolvus alkaline granites/rhyolites; 1c-d-e, silica over/under-saturated alkaline/peralkaline syenites/trachytes; 1c, gem zircon in hawaiites and alkali basalts; 1e, 2, 3a-b-c, 4a-b-c, subsolvus alkaline granites/rhyolites; 4a-b-c, 5a-b-c, 6a-b, basic to intermediate calc-alkaline rocks (gabbros, diorites, tonalites, quartz diorites and andesites-dacites); 5a-b-c, calc-alkaline granites/rhyolites; 4a-b, 5a-b-c, high-K calc-alkaline, or Mg-K granites/rhyolites; 4c, 5a-b-c, subalkaline, or Fe–K granites/rhyolites; 3b-c, 4b-c, 5b-c, 6a-b, peraluminous porphyritic granites/rhyolites; 3c, 4c, 5c, 6a, peraluminous leucogranites; 3c, 4c, 5c, 6a, autochthonous peraluminous granites and migmatites.

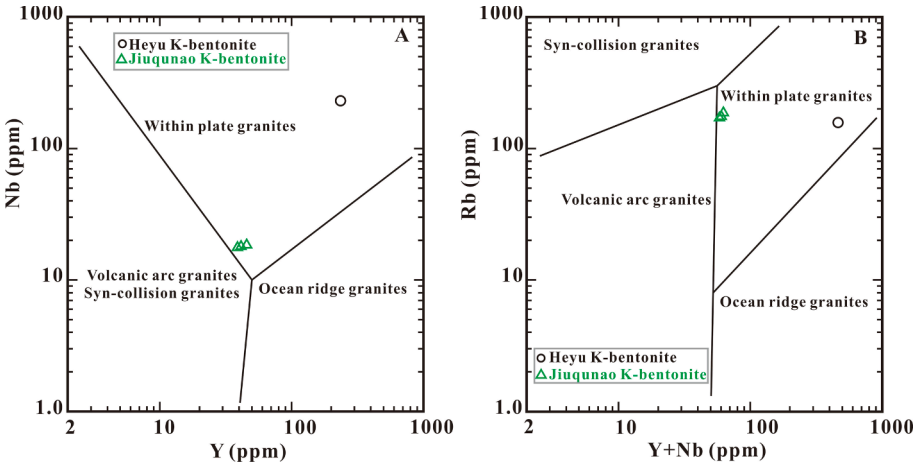

Fig. 12. Plots (Pearce et al., 1984) of Nb *versus* Y and Rb *versus* (Y + Nb) for the K-bentonites in the Doushantuo cap dolostone in South China.

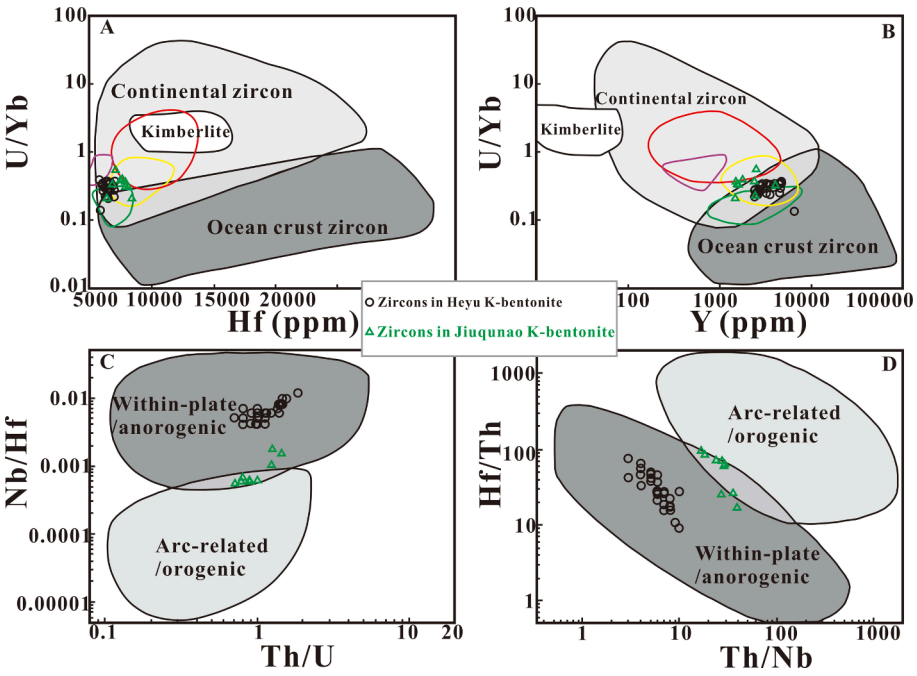

Fig. 13. Zircon Hf-U/Yb, Y-U/Yb, Th/U-Nb/Hf and Th/Nb-Hf/Th diagrams (Grimes et al., 2007; Gao et al., 2013 and references therein; Hawkesworth and Kemp, 2006; Yang et al., 2012) for the volcanic zircons in the K-bentonites in the Doushantuo cap dolostone from South China, distinguishing the possible tectonic setting of the volcanism that produced the zircons. Red circles represent zircons from felsic rocks at convergent continental margins before post-collision extension; yellow circles, zircons from basalts and rhyolites in post-collision extensional setting; green circles, zircons from *meta*-gabbros from divergent continental margin; purple circles, zircons from basalts in intra-continental rifts.

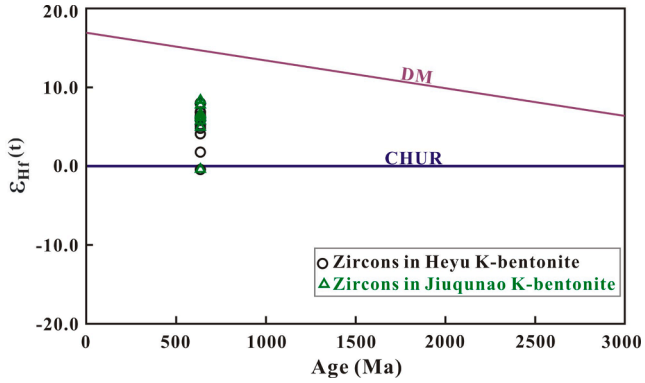

Fig. 14. $\varepsilon_{Hf}(t)$ *versus* age diagram for the volcanic zircons in the Doushantuo cap dolostone from South China.

discovered in the Jiuqunao, Huajipo and Jiulongwan sections in the platform, and in the Lantian section in the slope (Condon et al., 2005; Yin et al., 2005; Wan et al., 2013; Xing et al., 2018). Thus it implies that the volcanic ashes from the young volcanic episode may have covered a wider area.

Three mainly possible models for the sedimentary sequence of the Marinoan cap dolostones from basin to platform have been proposed (Fig. 1; Jiang et al., 2006; Hoffman et al., 2007), and the distribution of the K-bentonites in the Doushantuo cap dolostones in South China may possess a link with one of them. Based on the above clarification of the volcanic eruption episodes represented by the K-bentonites and the distribution characteristics of them, the following three possible relationships between the distribution of the K-bentonites and the sedimentary sequence model of the cap dolostones could be inferred (Fig. 1). (1) Assuming that the deposition of the Marinoan cap dolostones is isochronous (Fig. 1A), there would be such a possibility. A small-scale volcanic eruption represented by the K-bentonite from the Heyu section occurred first, and the volcanic ashes covered merely the Heyu area. Then, a large-scale volcanic eruption represented by the K-bentonite from the Jiuqunao section took place, and the ashes may have covered a larger area in the northern part of the Yangtze Platform. This assumption is not well consistent with the fact that the younger K-bentonite, which should have had a wider coverage area, has not been found in the cap dolostone deposited in the deep-water realm (the Heyu area) of the northern Yangtze Platform. (2) If the deposition of the Marinoan cap dolostones is semi-diachronous (Fig. 1B), then there may be the following possibilities. An episode of volcanic eruption represented by the older K-bentonite occured first, and its scale was limited, then the ashes only covered the Heyu area. Or this episode of volcanic eruption had a large scale, but its eruption time was synchronous with that the cap dolostone began to deposit in the basin of the northern Yangtze Platform. Therefore, the ashes could only be preserved in the early deposition of the cap dolostone in the basin of the northern Yangtze Platform (the Heyu area). Later, there was a large-scale volcanic eruption represented by the K-bentonite from the Jiuqunao section, the ashes may have covered a large area of the northern part of the Yangtze Platform. This assumption is also not well consistent with the fact that the younger K-bentonite, which should have had a wider coverage area, has not been discovered in the cap dolostone deposited in the deep-water realm (the Heyu area) of the northern Yangtze Platform. (3) If the deposition of the Marinoan cap dolostones is diachronous (Fig. 1C), then the following possibilities may exist. An episode of volcanic eruption represented by the older K-bentonite occured first, and its scale was limited, then the ashes only covered the Heyu area. Or this episode of volcanic eruption had a large scale, but its eruption time was synchronous with that the cap dolostone began to deposit in the basin of the northern Yangtze Platform. Therefore, the ashes could only be preserved in the early deposition of the cap dolostone in the basin of the northern Yangtze Platform (the Heyu area). Later, there was a large-scale volcanic eruption represented by the K-bentonite from the Jiuqunao section, the ashes may have covered a large area of the northern part of the Yangtze Platform. Therefore, K-bentonites representing eruption of this episode can be found in the cap dolostones of many sections (Jiuqunao, Huajipo, Jiulongwan, Lantian, etc.) in the platform interior and slope of the Yangtze Platform. However, it is impossible to discover K-bentonites of this episode in the cap dolostones in the basin of the northern Yangtze Platform (the Heyu area). The reason is that they are most probably preserved in the adjacent strata (limestones interbedded with shales) overlying the cap dolostones from this region. If this hypothesis is correct, then it is expected to find the young K-bentonites in the strata

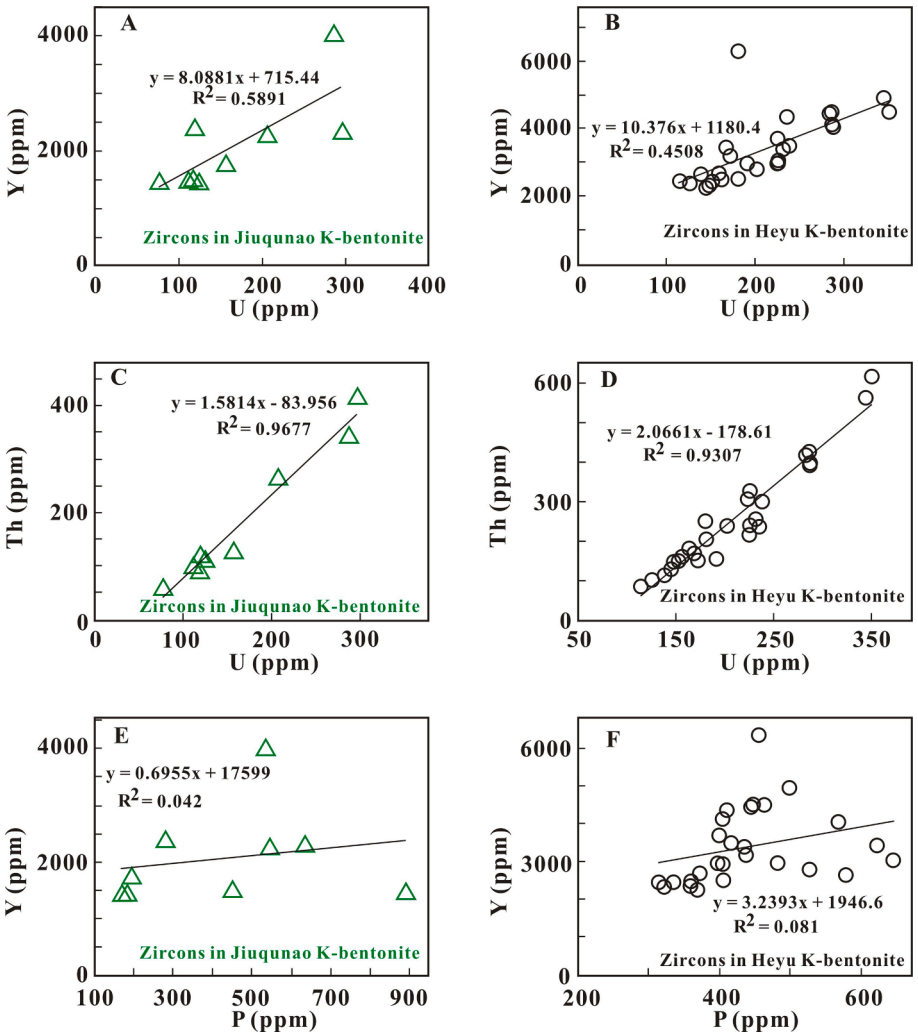

Fig. 15. Correlation plots of U *versus* Y, U *versus* Th and P *versus* Y for the volcanic zircons from the K-bentonites in the Doushantuo cap dolostone in South China.

immediately overlying the cap dolostones in the basin of the northern Yangtze Platform. This expectation remains to be tested by the discovery of K-bentonites in the future.

The three possible sedimentary models of the Marinoan cap dolostones (Fig. 1) will lead to a different understanding of the relationship between the timescale of the cap dolostone and the ice-sheet meltdown time (Hoffman et al., 2007). Therefore, whichever the above possible connections is consistent with the geological fact, the clarification of two episodes of volcanic eruptions represented by K-bentonites in the Doushantuo cap dolostones from South China, undoubtedly remind that high-precision U-Pb geochronological study (in preparation) on zircons in the K-bentonite in the cap dolostones from the basin of the northern Yangtze Platform, has potential significance for the duration constraint (Sui et al., 2018) and genetic interpretation of the Marinoan cap dolostone, even for the test of the snowball Earth hypothesis.

6. Conclusions

The following conclusions have been drawn based on whole-rock and zircon geochemical studies on the K-bentonites in the Doushantuo cap dolostones in South China.

(1) The primary magmas of the K-bentonites in the Doushantuo cap dolostones from the Jiuqunao and Heyu sections are different in nature, and are rhyodacitic (dacitic) and pantelleritic (comenditic), respectively.

(2) The source volcanoes of the K-bentonites in the Doushantuo cap dolostones are more likely to occur in the extensional setting on the northern margin of the Yangtze Block. The source magmas of the K-bentonites are mainly mantle-derived, and may have mixed with the crustal materials from the northern margin of the Yangtze Block.

(3) Two episodes of the source volcanic eruptions of the K-bentonites in the Doushantuo cap dolostones could be identified. The K-bentonite from the Heyu section most probably represents the record of volcanic eruption of the old episode, while the K-bentonite from the Jiuqunao section represents that of the young episode. The here proposed dual episodic deposition of K-bentonites within the Doushantuo cap carbonates holds potential significance to constrain 1) the duration of the cap carbonate deposition and 2) their genesis in potential slushball or snowball Earth environments.

CRediT authorship contribution statement

Mingzhong Zhou: Funding acquisition, Conceptualization, Investigation, Formal analysis, Writing – original draft, Writing – review & editing. **Bin Wan:** Investigation, Writing – review & editing. **Li Zhou:** Writing – review & editing. **Enlin Yang:** Writing – review & editing. **Liansheng Yang:** Writing – original draft. **Taiyi Luo:** Investigation, Writing – review & editing.

Declaration of Competing Interest

The authors declare that they have no known competing financial interests or personal relationships that could have appeared to influence the work reported in this paper.

Acknowledgements

We would like to thank Simon Hohl and an anonymous reviewer for their thorough and very thoughtful reviews and comments that greatly improved this manuscript. We are indebted to Yuwei Deng of the Shale Gas Evaluation and Exploitation Key Laboratory of Sichuan Province of China for technical supports of XRD analyses, Yan Huang, Nengping Shen, Zhihui Dai, Youwei Chen, and Tingguang Lan of the State Key Laboratory of Ore Deposit Geochemistry, Institute of Geochemistry, Chinese Academy of Sciences for technical supports of XRF, ICP-MS, LA-ICP-MS and LA-MC-ICP-MS analyses, Shengying Yang for assistance in preparation for the early draft of this manuscript, and Fang Li and Junjie Zhou for assistance in sample collections. This work was supported by the first-class discipline group of geography of Guizhou Province (No. [2019]125), the National Natural Science Foundation of China (41462001, 40963002) and the Project of National Key Research and Development Program of China (2016YFC0502601).

References

Allen, P.A., Etienne, J.L., 2008. Sedimentary challenge to Snowball Earth. Nautre Geoscience 1 (12), 817–825.

Ao, W., Zhang, Y., Zhang, R., Zhao, Y., Sun, Y., 2014. Neoproterozoic crustal accretion of the northern margin of Yangtze plate: Constrains from geochemical characteristics, LA-ICP-MS zircon U-Pb chronology and Hf isotopic compositions of trondhjemite from Zushidian area, Hannan region. Geol. Rev. 60, 1393–1408 (in Chinese with English abstract).

Belousova, E., Griffin, W., O'Reilly, S.Y., Fisher, N., 2002. Igneous zircon: trace element composition as an indicator of source rock type. Contrib. Miner. Petrol. 143 (5), 602–622.

Blichert-Toft, J., Albarède, F., 1997. The Lu-Hf isotope geochemistry of chondrites and the evolution of the mantle-crust system. Earth Planet. Sci. Lett. 148 (1-2), 243–258.

Chu, Z., He, H., Ramezani, J., Bowring, S.A., Hu, D., Zhang, L., Zheng, S., Wang, X., Zhou, Z., Deng, C., Guo, J., 2016. High-precision U-Pb geochronology of the Jurassic Yanliao Biota from Jianchang (western Liaoning Province, China): Age constraints on the rise of feathered dinosaurs and eutherian mammals. Geochem. Geophys. Geosyst. 17 (10), 3983–3992.

Condon, D., Zhu, M., Bowring, S., Wang, W., Yang, A., Jin, Y., 2005. U-Pb ages from the Neoproterozoic Doushantuo Formation, China. Science 308, 95–98.

De Biévre, P., Taylor, P.D.P., 1993. Table of the isotopic compositions of the elements. Int. J. Mass Spectrom. Ion Process. 123 (2), 149–166.

Fang, Q., Churchman, G.J., Hong, H., Chen, Z.-Q., Liu, J., Yu, J., Han, W., Wang, C., Zhao, L., Furnes, H., 2017. New insights into microbial smectite illitization in the Permo-Triassic boundary K-bentonites, South China. Appl. Clay Sci. 140, 96–111.

Gao, Q., Zhang, N., Xia, W., Feng, Q., Chen, Z.-Q., Zheng, J., Griffin, W.L., O'Reilly, S.Y., Pearson, N.J., Wang, G., Wu, S., Zhong, W., Sun, X., 2013. Origin of volcanic ash beds across the Permian-Triassic boundary, Daxiakou, South China: Petrology and U-Pb age, trace elements and Hf-isotope composition of zircon. Chem. Geol. 360-361, 41–53.

Ge, X., Mou, C., Wang, C., Men, X., Chen, C., Hou, Q., Somerville, I.D., 2019. Mineralogical and geochemical characteristics of K-bentonites from the Late Ordovician to the Early Silurian in South China and their geological significance. Geol. J. 54 (1), 514–528.

Gong, N., Hong, H., Huff, W.D., Fang, Q., Bae, C.J., Wang, C., Yin, K., Chen, S., 2018. Influences of sedimentary environments and volcanic sources on diagenetic alteration of volcanic tuffs in South China. Sci. Rep. 8, 7616.

Goolaerts, A., Mattielli, N., de Jong, J., Weis, D., Scoates, J.S., 2004. Hf and Lu isotopic reference values for the zircon standard 91500 by MC-ICP-MS. Chem. Geol. 206 (1-2), 1–9.

Griffin, W.L., Wang, X., Jackson, S.E., Pearson, N.J., O'Reilly, S.Y., Xu, X., Zhou, X., 2002. Zircon chemistry and magma mixing, SE China: In-situ analysis of Hf isotopes, Tonglu and Pingtan igneous complexes. Lithos 61 (3-4), 237–269.

Grimes, C.B., John, B.E., Kelemen, P.B., Mazdab, F.K., Wooden, J.L., Cheadle, M.J., Hanghøj, K., Schwartz, J.J., 2007. Trace element chemistry of zircons from oceanic crust: A method for distinguishing detrital zircon provenance. Geology 35 (7), 643. https://doi.org/10.1130/G23603A.110.1130/2007159.

Grotzinger, J.P., Knoll, A.H., 1995. Anomalous carbonate precipitates: is the Precambrian the key to the Permian? Palaios 10, 578–596.

Guo, W., Su, W., Zhang, J., Li, H., Zhou, H., Li, H., Ettensohn, F.R., Huff, W.D., 2019. Zircon U-Pb dating and Hf isotopes of K-bentonites from the Tieling Formation in a new exposure of the Jixian Section, Tianjin, North China Craton. Acta Petrolog. Sinica 35, 2433–2454 (in Chinese with English abstract).

Hawkesworth, C.J., Kemp, A.I.S., 2006. Using hafnium and oxygen isotopes in zircons to unravel the record of crustal evolution. Chem. Geol. 226 (3-4), 144–162.

Hoffman, P.F., Halverson, G.P., Domack, E.W., Husson, J.M., Higgins, J.A., Schrag, D.P., 2007. Are basal Ediacaran (635 Ma) post-glacial "cap dolostones" diachronous? Earth Planet. Sci. Lett. 258, 114–131.

Hoffman, P.F., Kaufman, A.J., Halverson, G.P., Schrag, D.P., 1998. A Neoproterozoic snowball Earth. Science, 281: 1342-1346.

Hohl, S.V., Becker, H., Jiang, S.-Y., Ling, H.-F., Guo, Q., Struck, U., 2017. Geochemistry of Ediacaran cap dolostones across the Yangtze Platform, South China: implications for diagenetic modification and seawater chemistry in the aftermath of the Marinoan glaciation. J. Geol. Soc. 174 (5), 893–912.

Hong, H., Algeo, T.J., Fang, Q., Zhao, L., Ji, K., Yin, K.e., Wang, C., Cheng, S., 2019a. Facies dependence of the mineralogy and geochemistry of altered volcanic ash beds: An example from Permian-Triassic transition strata in southwestern China. Earth Sci. Rev. 190, 58–88.

Hong, H., Zhao, L., Fang, Q., Algeo, T.J., Wang, C., Yu, J., Gong, N., Yin, K.e., Ji, K., 2019b. Volcanic sources and diagenetic alteration of Permian-Triassic boundary K-bentonites in Guizhou Province, South China. Palaeogeogr. Palaeoclimatol. Palaeoecol. 519, 141–153.

Huff, W.D., 2016. Review K-bentonites: A review. Am. Mineral. 101 (1), 43–70.

Huff, W.D., Bergstrom, S.M., Kolata, D.R., 2000. Silurian K-bentonites of the Dnestr Basin, Podolia, Ukraine. Journal of the Geological Society, London, 157: 493-504.

Hyde, W.T., Crowley, T.J., Baum, S.K., Peltier, W.R., 2000. Neoproterozoic 'snowball Earth' simulations with a coupled climate/ice-sheet model. Nature 405 (6785), 425–429.

Jiang, G., Kennedy, M.J., Christie-Blick, N., 2003. Stable isotopic evidence for methane seeps in Neoproterozoic postglacial cap carbonates. Nature 426 (6968), 822–826.

Jiang, G., Kennedy, M.J., Christie-Blick, N., Wu, H., Zhang, S., 2006. Stratigraphy, sedimentary structures, and textures of the late Neoproterozoic Doushantuo cap carbonate in South China. J. Sediment. Res. 76 (7), 978–995.

Kennedy, M.J., Christie-Blick, N., Sohl, L.E., 2001. Are Proterozoic cap carbonates and isotopic excursions a record of gas hydrate destabilization following Earth's coldest intervals? Geology 29 (5), 443. https://doi.org/10.1130/0091-7613(2001)029<0443:APCCAI>2.0.CO;2.

Kirschvink, J.L., 1992. Late Proterozoic low-latitude global glaciation: The snowball Earth. In The Proterozoic Biosphere: A Multidisciplinary Study (J.W. Schopf and C. Klein, Eds.), pp. 51-52.

Lewis, J.P., Weaver, A.J., Eby, M., 2007. Snowball versus slushball Earth: Dynamic versus nondynamic sea ice? J. Geophys. Res. 112, C11014.

Li, X.-H., Li, W.-X., Li, Z.-X., Lo, C.-H., Wang, J., Ye, M.-F., Yang, Y.-H., 2009. Amalgamation between the Yangtze and Cathaysia Blocks in South China: Constraints from SHRIMP U-Pb zircon ages, geochemistry and Nd–Hf isotopes of the Shuangxiwu volcanic rocks. Precambr. Res. 174 (1-2), 117–128.

Liu, YongSheng, Hu, ZhaoChu, Zong, KeQing, Gao, ChangGui, Gao, S., Xu, J., Chen, HaiHong, 2010. Reappraisement and refinement of zircon U-Pb isotope and trace element analyses by LA-ICP-MS. Chin. Sci. Bull. 55 (15), 1535–1546.

Liu, Y., Hu, Z., Gao, S., Günther, D., Xu, J., Gao, C., Chen, H., 2008. In situ analysis of major and trace elements of anhydrous minerals by LA-ICP-MS without applying an internal standard. Chem. Geol. 257 (1-2), 34–43.

Ludwig, K.R., 2003. User's Manual for Isoplot 3.00: A geochronological toolkit for Microsoft excel. Berkeley Geochronological Center Special Publication, No. 4, pp. 25–32.

McDonough, W.F., Sun, S.-s., 1995. The composition of the Earth. Chem. Geol. 120 (3-4), 223–253.

Micheels, A., Montenari, M., 2008. A snowball Earth versus a slushball Earth: Results from Neoproterozoic climate modeling sensitivity experiments. Geosphere 4 (2), 401. https://doi.org/10.1130/GES00098.1.

Moore, D.M., Reynolds, R.C., 1997. X-ray diffraction and the identification and analysis of clay minerals. Oxford University Press, New York, p. 378.

PEARCE, J.A., HARRIS, N.B.W., TINDLE, A.G., 1984. Trace element discrimination diagrams for the tectonic interpretation of granitic rocks. J. Petrol. 25 (4), 956–983.

Pupin, J.P., 2000. Granite genesis related to geodynamics from Hf-Y in zircon. Transactions of the Royal Society of Edinburgh: Earth Sciences, 91: 245-256.

Scherer, E., Munker, C., Mezger, K., 2001. Calibration of the Lutetium-Hafnium clock. Science 293, 683–687.

Shields, G.A., 2005. Neoproterozoic cap carbonates: a critical appraisal of existing models and the plumeworld hypothesis. Terra Nova 17 (4), 299–310.

Shnukov, S.E., Andreev, A.V., Savenok, S.P., 1997. Admixture elements in zircons and apatite: a tool for provenances studies of terrigenous sedimentary rocks. European Union of Geosciences.

Song, S., Yang, L., Zhang, Y., Niu, Y., Wang, C., Su, L.i., Gao, Y., 2017. Qi-Qin Accretionary Belt in Central China Orogen: accretion by trench jam of oceanic plateau and formation of intra-oceanic arc in the Early Paleozoic Qin-Qi-Kun Ocean. Sci. Bull. 62 (15), 1035–1038.

Spence, G.H., Le Heron, D.P., Fairchild, I.J., 2016. Sedimentological perspectives on climatic, atmospheric and environmental change in the Neoproterozoic Era. Sedimentology 63, 253–306.

Su, W., He, L., Wang, Y., Gong, S., Zhou, H., 2003. K-bentonite beds and high-resolution integrated stratigraphy of the uppermost Ordovician Wufeng and the lowest Silurian Longmaxi formations in South China. Sci. China (Series D) 46 (11), 1121–1133.

Su, W., Huff, W.D., Ettensohn, F.R., Liu, X., Zhang, Ji'en, Li, Z., 2009. K-bentonite, black-shale and flysch successions at the Ordovician-Silurian transition, South China: Possible sedimentary responses to the accretion of Cathaysia to the Yangtze Block and its implications for the evolution of Gondwana. Gondwana Res. 15 (1), 111–130.

Su, WenBo, Li, HuaiKun, Huff, W.D., Ettensohn, F.R., Zhang, ShiHong, Zhou, HongYing, Wan, YuSheng, 2010. SHRIMP U-Pb dating for a K-bentonite bed in the Tieling Formation, North China. Chin. Sci. Bull. 55 (29), 3312–3323.
Su, W., Zhang, S., Huff, W.D., Li, H., Ettensohn, F.R., Chen, X., Yang, H., Han, Y., Song, B., Santosh, M., 2008. SHRIMP U-Pb ages of K-bentonite beds in the Xiamaling Formation: Implications for revised subdivision of the Meso- to Neoproterozoic history of the North China Craton. Gondwana Res. 14 (3), 543–553.
Sui, Y.u., Huang, C., Zhang, R., Wang, Z., Ogg, J., Kemp, D.B., 2018. Astronomical time scale for the lower Doushantuo Formation of early Ediacaran, South China. Sci. Bull. 63 (22), 1485–1494.
Tang, H., Zhao, Z., Huang, R., Han, Y., Su, Y., 2008. Primary Hf isotopic study on zircons from the A-type granites in eastern Junggar of Xinjiang, Northwest China. Acta Mineralogica Sinica 28, 335–342 (in Chinese with English abstract).
Tao, H., Wang, Q., Li, X., He, H., 1985. Preliminary analysis of the structures in the rift system at the northern margin of the Yangtze platform. Regional Geol. China 13, 96–104 (in Chinese with English abstract).
Vervoort, J.D., Blichert-Toft, J., 1999. Evolution of the depleted mantle: Hf isotope evidence from juvenile rocks through time. Geochim. Cosmochim. Acta 63 (3-4), 533–556.
Wan, B., Guan, C., Zhou, C., Meng, F., Pang, K., Tang, Q., Rao, X., 2013. Petrologic and geochemical characteristics of K-bentonites from the basal Ediacaran in Yangtze Platfrom, South China and their geological significance. Acta Petrol. Sinica 29, 4373–4386 (in Chinese with English abstract).
Wang, H., Li, Z., Liu, S., Ran, B.o., Song, J., Li, J., Ye, Y., Li, N., 2020a. Ediacaran extension along the northern margin of the Yangtze Platform, South China: Constraints from the lithofacies and geochemistry of the Doushantuo Formation. Mar. Pet. Geol. 112, 104056. https://doi.org/10.1016/j.marpetgeo.2019.104056.
Wang, J., Li, Z., 2003. History of Neoproterozoic rift basins in South China: implications for Rodinia break-up. Precambr. Res. 122, 141–158.
Wang, W., Zhou, C., Guan, C., Yuan, X., Chen, Z., Wan, B., 2014. An integrated carbon, oxygen, and strontium isotopic studies of the Lantian Formation in South China with implications for the Shuram anomaly. Chem. Geol. 373, 10–26.
Wang, W., Zhou, M., Chu, Z., Xu, J., Li, C., Luo, T., Guo, J., 2020b. Constraints on the Ediacaran-Cambrian boundary in deep-water realm in South China: Evidence from zircon CA-ID-TIMS U-Pb ages from the topmost Liuchapo Formation. Sci. China Earth Sci. 63 (8), 1176–1187.
Wang, X., Pupin, J.P., 1992. Distribution characteristics of trace elements in zircons from granitic rocks. Scientia Geol. Sinica 2, 131–140 (in Chinese with English abstract).
Watson, E.B., 1979. Zircon saturation in felsic liquids: Experimental results and applications to trace element geochemistry. Contrib. Miner. Petrol. 70 (4), 407–419.
White, J.C., Parker, D.F., Ren, M., 2009. The origin of trachyte and pantellerite from Pantelleria, Italy: Insights from major element, trace element, and thermodynamic modeling. J. Volcanol. Geoth. Res. 179, 33–55.
Wiedenbeck, M., Alle, P., Corfu, F., Griffin, W.L., Meier, M., Oberli, F., Von Quadt, A., Roddick, J.C. and Spiegel, W., 1995. Three natural zircon standards for U-Th-Pb, Lu-Hf, trace element and REE analyses. Geostandards Newsletter, 19: 1-23.
Winchester, J.A., Floyd, P.A., 1977. Geochemical discrimination of different magma series and their differentiation products using immobile elements. Chem. Geol. 20, 325–343.
Xing, L., Luo, T., Huang, Z., Qian, Z., Zhou, M., He, H., 2018. U-Pb zircon age of the base of the Ediacaran System at the southern margin of the Qinling Orogen. Acta Geochimica 37 (3), 414–421.
Xu, J., Wu, H., Chu, Z., Fang, Q., Zhang, S., Yang, T., Li, H., Somerville, I., 2020. Geochemistry and U-Pb geochronology of K-bentonites from the Pingliang Formation of the Upper Ordovician in Gansu, North China, and their tectonic implications. Geol. J. 55 (5), 3522–3536.
Yang, J., Cawood, P.A., Du, Y., Huang, H.u., Huang, H., Tao, P., 2012. Large Igneous Province and magmatic arc sourced Permian-Triassic volcanogenic sediments in China. Sed. Geol. 261-262, 120–131.
Yin, C., Tang, F., Liu, Y., Gao, L., Liu, P., Xing, Y., Yang, Z., Wan, Y., Wang, Z., 2005. U-Pb zircon age from the base of the Ediacaran Doushantuo Formation in the Yangtze Gorges, South China: constraint on the age of Marinoan glaciation. Episodes 28 (1), 48–51.
Yin, Y., Gao, Y., Wang, P., Qu, X., Liu, H., 2019. Discovery of Triassic volcanic-sedimentary strata in the basement of Songliao Basin. Science Bulletin 64 (10), 644–646.
Zhang, G., Meng, Q., Yu, Z., Sun, Y., Zhou, D., Guo, A., 1996. Orogenesis and dynamics of the Qingling Orogen. Science in China (Series D) 39, 225–234.
Zhou, C., Bao, H., Peng, Y., Yuan, X., 2010. Timing the deposition of O-depleted barite at the aftermath of Nantuo glacial meltdown in South China. Geology 38, 903–906.
Zhou, C., Huyskens, M.H., Lang, X., Xiao, S., Yin, Q.-Z., 2019. Calibrating the terminations of Cryogenian global glaciations. Geology 47 (3), 251–254.
Zhou, C., Tucker, R., Xiao, S., Peng, Z., Yuan, X., Chen, Z., 2004. New constraints on the ages of Neoproterozoic glaciations in south China. Geology 32 (5), 437. https://doi.org/10.1130/G20286.110.1130/2004072.
Zhou, MingZhong, Luo, TaiYi, Li, ZhengXiang, Zhao, H., Long, HanSheng, Yang, Y., 2008. SHRIMP U-Pb zircon age of tuff at the bottom of the Lower Cambrian Niutitang Formation, Zunyi, South China. Chin. Sci. Bull. 53 (4), 576–583.
Zhou, MingZhong, Luo, TaiYi, Liu, ShiRong, Qian, ZhiKuan, Xing, LeCai, 2013. SHRIMP zircon age for a K-bentonite in the top of the Laobao Formation at the Pingyin section, Guizhou, South China. Science China Earth Sciences 56 (10), 1677–1687.
Zhou, M., Luo, T., Huff, W.D., Liu, S., 2014. Prominent lower Cambrian K-Bentonites in South China: Distribution, Mineralogy, and Geochemistry. J. Sediment. Res. 84 (10), 842–853.
Zhou, M., Luo, T., Huff, W.D., Yang, Z., Zhou, G., Gan, T., Yang, H., Zhang, D.i., 2018. Timing the termination of the Doushantuo negative carbon isotope excursion: evidence from U-Pb ages from the Dengying and Liuchapo formations, South China. Science Bulletin 63 (21), 1431–1438.